

Effects of gravitational lens models on merging Binary Black Hole systems

A thesis submitted to the University of Glasgow for the degree of
Master of Science (MSc) in Astrophysics
in the College of Science and Engineering

September 2020

XXX
Institute for Gravitational Research
School of Physics and Astronomy
Under the supervision of Dr. Christopher Messenger

*The important thing is not to stop questioning
Curiosity has its own reason for existing
~Albert Einstein*

Contents

Contents	2
List of figures	4
List of tables	5
Abstract	6
Acknowledgements	7
1 Introduction	8
1.1 Why Binary Black Hole mergers?	9
1.2 Gravitational Lens Models	10
1.3 Wave Optics and Geometric Optics limit	10
1.4 Organization of the scientific report	11
2 Theoretical Framework	13
2.1 Wave Optics in Gravitational Lensing.....	13
2.1.1 Geometric Optics Approximation	16
2.2 Point Mass Lens	16
2.3 Singular Isothermal Sphere Lens	18
2.4 Magnitude of the Amplification Factor	19
2.5 Phase of the Amplification Factor	21
2.6 Transition between geometric and wave optics limit.....	23
3 Statistical and Computational Methods	26
3.1 Bayesian methods of parameter estimation.....	26
3.1.1 Bayes Factor and Bayesian evidence	26
3.2 Nested Sampling.....	27
3.2.1 Dynesty – Nested Sampling Algorithm	27
3.3 Bilby – Bayesian Inference Library	27
3.4 LALSuite – LIGO gravitational wave analysis algorithm	28
4 Source Signal	29
4.1 Sine-Gaussian Signal	29
4.2 Binary Black Hole merger Gravitational wave signal	31
5 Results & Analysis	34
5.1 Source signal parameters before lensing by the Point-mass object.....	34
5.1.1 Sine-Gaussian signal.....	34
5.1.2 BBH merger signal.....	35
5.2 Source signal parameters after lensing by the Point-mass object.....	37
5.2.1 Sine-Gaussian signal.....	37
5.2.2 BBH merger signal.....	39
5.3 Strong and weak gravitational lensing	41
5.4 Sampling without considering the lens effect.....	41
6 Conclusion	43
6.1 Summary.....	43
6.2 Conclusion	44
6.3 Future scope of the research	44
References.....	45
Appendices	48
Appendix A	48
Appendix B	49
Appendix C	50

Word Count: 11449

Page Count: 37

List of figures

2.1	Gravitational lens geometry.....	14
2.2	Magnitude of amplification factor versus dimensionless frequency.	20
2.3	Magnitude of amplification factor versus source position.	21
2.4	Phase of amplification factor versus dimensionless frequency.....	22
2.5	Phase of the amplification factor versus source position.....	23
2.6	Transition between wave and geometric optics limit	23
2.7	Surface plots of Magnitude of Amplification factor in two limits.	24
4.1	Sine-Gaussian lensed and unlensed source signal.....	30
4.2	BBH merger lensed and unlensed source signal.....	32
5.1	Sine-Gaussian unlensed signal parameters' corner plots.....	35
5.2	BBH merger unlensed signal parameters' corner plots.....	36
5.3	Sine-Gaussian lensed signal parameters' corner plots.	37
5.4	BBH merger lensed signal parameters' corner plots.	40
5.5	BBH merger signal parameters' corner plots ignoring lensing effects.....	41

List of tables

2.1	Comparison of lensing parameters for point-mass and SIS lens models.	19
4.1	Lensing and signal injection parameters of Sine-Gaussian signal.....	31
4.2	Lensing and signal injection parameters of BBH merger signal.....	33
5.1	Prior and posterior values of unlensed sine-gaussian signal.....	34
5.2	Prior and posterior values of unlensed BBH merger signal.	36
5.3	Prior and posterior values of lensed sine-gaussian signal.	38
5.4	Prior and posterior values of lensed BBH merger signal.	39

ABSTRACT

This scientific research explores the nature and properties of a lensed gravitational wave signal resulting from compact binary coalescence of merging binary black hole system. In the first part of the research, we focus on the theoretical analysis performed over the past years based on the Takahashi-Nakamura formalism to analytically express the amplification obtained in the source signal due to its encounter with a compact isolated astrophysical lens object. This research presents the results on both wave optics and geometric optics limit and produces an ideal transition point between the two limits for a varying dimensionless frequency of the source signal. We observe that for any value of the dimensionless frequency greater than unity, both the limits hold well and produce similar amount of magnification. In the second part of the research, we produce a sine-gaussian source model and analyze how the source properties are affected by the presence of a point-mass lens model on its way to the observer which results in a strong lensing phenomenon. We see no correlation between the frequency of the sine-gaussian wave and the lensing parameters, but solid correlation between the amplitude of the signal, the source position offset with the lens and lens mass. In the final part of the research, we model a binary black hole merger GW signal and observe how a point-mass lens model would affect the nature and physical parameters of the merging binary black hole system. We see strong correlation between the luminosity distance and lensing parameters. When we create a strongly lensed signal and perform parameter estimation using nested sampling by assuming that there is no lensing, we simulate how LIGO/VIRGO samples any incoming GW signal. We can clearly see that the resulting posteriors of source parameters have huge offset from the originally injected values because of ignoring the lensing effect on the input side. This leads to a conclusion that for GW signals which have higher probability of strong lensing, the interferometers should consider lensing effects while sampling any incoming gravitational wave signal during its observing runs.

Acknowledgements

I wish to express my sincere gratitude to my supervisor *Dr. Christopher Messenger* from the Institute for Gravitational Research, School of Physics and Astronomy, College of Science and Engineering, University of Glasgow whose knowledge has been a sheer catalyst throughout this research project. His brilliance, suggestions and advises in programming and statistical methods have been a spirit of excellence in realizing the goals of this project and achieving them within a short span of three months.

I am deeply thankful to *Prof. Graham Woan and my supervisor* for providing me with the theoretical acquaintance to Statistical Astronomy as a part of my MSc coursework and *Prof. Martin Hendry* for always being supportive as the Head of School and for all his useful discussions in the field of gravitational waves and gravitational lensing.

Dr. Johannes Courtial, the MSc project coordinator have my thanks for passing information regarding remote workings, deadlines and oral presentations and being accommodative to all the student requests on time. I also thank *him* and *Dr. Iain Martin* for marking my interim oral presentation and for their valuable comments and feedback.

I am grateful to all the *other teaching and research staffs* in the School of Physics and Astronomy for helping me with academic and research related matters.

I would also like to thank the entire *IGR Data Analysis team* (academic and research staffs, PhD students and Researchers) for their generous comments and suggestions and for taking active interest in my work every week during our group meetings throughout the tenure of my MSc thesis work.

I would like to extend my thank you to *Prof. Sara Ellison* from University of Victoria, Canada for introducing me to astronomy research in the first place during my summer research as a part of the Mitacs Globalink fellowship program.

I also thank my *flat mates, course mates and friends* from Glasgow, UK and Chennai, India for being a moral support during the COVID-19 pandemic lockdowns and mutually helping me out during the remote working period.

Ultimately, I would like to present my thanks to *my father Mr. R. Viswanathan and the rest of my family* for believing in my interest and expertise in Astronomy and supporting me throughout the MSc coursework, financially and morally.

Chapter 1

Introduction

Albert Einstein's publication on Theory of General Relativity (Einstein 1915) has made it possible to describe many astrophysical phenomena that couldn't be explained by classical Newtonian physics. One such phenomena that was successfully described by Einstein's theory of relativity was gravitational lensing. Einstein's theory describes how the concentration of mass into compact objects distorts the space that surrounds them. This theory also successfully explained the deflection of light mechanism in 1919. Null geodesics are obeyed by light rays in space time curvature and the deflection occurs by the gravitational potential of the massive lens object in-between the source and the observer. Gravitational lensing is one of the most interesting phenomena in the regime of gravitational wave (further referred as GW) research and astrophysics. This phenomena occurs when light emitted by any distant sources like galaxies, stars, neutron stars travel along the space and reach the observer (interferometers, in our case), but on its way, light rays from the source gets distorted and changes direction (bending of light occurs) because of its encounter with any massive astronomical objects like galactic halos, black holes etc. (Pacsyoski 1986) This bending of light causes momentary brighter appearance of the source by a certain magnitude because it is amplified by the gravitational pull of the lensing object. (Liao 2019, Takahashi & Nakamura 2003, T.R. 2006)

The gravitational lensing phenomena majorly depends on the properties of the lens that bend the light from the source. (Paolis 2002) Several thousand gravitational lensing of astronomical entities have been observed in the past century ever since 1919. (Bozza 2012, Diego 2019) With the recent Nobel prize winning detection of gravitational waves in 2015, the advancement of LIGO-VIRGO detectors (aLIGO, AdVIRGO) (Aasi 2015, Abbott 2019) and upcoming new detectors like Einstein Telescope and space bound interferometry detectors like Laser Interferometer Space Antenna (LISA), the number of such revolutionary gravitational lensing events in the regime of gravitational wave signal is expected to drastically increase.

Inspirals and binary mergers of compact objects such as black holes have a promising future not only in the field of gravitational waves but also in gravitational lensing. (Meena 2019, Nakamura 1997) When the gravitational waves from compact binary coalescence events pass through massive objects that can act as gravitational lens, then these gravitational waves will also bend, and lensing occurs just like it happens with light from a distant source. Gravitational lensing is usually treated as a phenomenon that occurs in geometric optics approximation limit. (Nakamura & Deguchi 1999) In case of gravitational waves being lensed, the wavelength is long and geometrics optics limit might not always prove to be valid at longer wavelengths. (Paolis 2001) If the wavelength becomes larger than the Schwarzschild radius of the lens mass M_L , then diffraction effect comes into play and the magnification in the amplitude of the gravitational wave due to lensing becomes small. The

ratio of M_L and λ is very important because this ratio determines the effect due to diffraction on lensing. This can be explained using the double slit experiment with the slit width approximately equal to Einstein's radius that is,

$$\xi_s \sim (M_L D)^{\frac{1}{2}} \quad (1.1)$$

where D is the distance between the slit and the screen of display. When waves of certain wavelength λ passes through this slit, it creates an interference pattern on the screen. Therefore, it is valid to say that the diffraction effect is important for

$$M_L \leq 10^8 M_\odot \left(\frac{f}{\text{mHz}} \right)^{-1} \quad (1.2)$$

where f is the frequency of the gravitational wave under consideration. The focused region by the gravitational lensing will have a relatively large area because of the diffraction effect and thus, the lensing probability will increase. (Ruffa 1999) The gravitational waves that are produced by compact binary coalescence events like binary black hole merger events are coherent. So, the interference effects should be considered important. Hence, we can expect that the wave effect will produce more information about the lensing process, the lens and the source under study.

1.1 Why Binary Black Hole mergers?

This research involves considering wave effects and geometric optics limit approximation in gravitational lensing of gravitational wave events. Gravitational waves are disruptions or ripples in space time curvature caused by massive objects creating energetic processes in the Universe. (Thorne 1983) The theoretical calculations by Einstein stated that these waves are caused by such massive objects and they travel in all directions at the speed of light carrying interesting information about the object, its origin and many other facts about the nature of gravity. On 14-September-2015, all the theoretical and mathematical modelling by Einstein was proved experimentally by the Nobel Prize winning discovery of gravitational waves from two merging binary black hole system that was approximately 1 billion light years away from Earth. (Abbott et al. 2016, Mclsaac 2019)

In this research, we primarily consider compact binary coalescence from binary black hole merger system as our primary target source of study for gravitational lensing effects. This is because inspirals and massive compact binary mergers are one of the most favorable gravitational wave sources (Singer 2019) as there are several examples of such detections in low mass category and in future, LISA and Einstein Telescope promises to detect gravitational waves from supermassive black hole mergers (in the mass range $10^5 - 10^9 M_\odot$) (Rhook 2005) and intermediate mass black hole mergers (in the mass range $10^2 - 10^5 M_\odot$) (Zhao 2005, Miller 2009). LISA will consider SMBH mergers as its primary source and detect them with high signal-to-noise-ratio (of approximately 10^3). The major hosts of supermassive black holes are the center of any galaxy. Thus, the search for SMBH mergers will mostly yield results at high redshifts when the central SMBH in any two distant galaxies tend to merge producing gravitational waves. (Futamase 1999) As the redshift will be high, there is more probability of lensing to occur when the gravitational wave travels towards the observer (i.e., earth or LISA). Hence, we can expect more gravitationally lensed

gravitational waves from such events in near future. Thus, binary black hole mergers in various mass ranges are encouraging candidates for this type of research on gravitational lensing due to gravitational wave events.

In strong gravitational lensing phenomenon, multi-lensing of the same event could be observed with a specific and viable time delays between each of them as we observe them in earth or space-based interferometers. The time delay is the key feature in strong lensing phenomena. (Haris 2018) This will be explained by the lens equation that describes the magnification produced due to the lensing phenomenon for a particular source offset and frequency of the GW radiation. The coalescing binary black hole mergers from Advanced LIGO and VIRGO are characterized by certain parameter sets like masses of each black hole, their spins, sky location, orientation and inclination with the observer etc. All these parameters may or may not be affected by the intervening massive object that act as the gravitational lens.

1.2 Gravitational Lens Models

Here we start by studying two simple gravitational lens models: (Takahashi and Nakamura 2003)

1. The point mass lens model
2. The SIS (Singular Isothermal Sphere) lens model

We start the study by calculating the amplification in the waveform due to gravitational lensing by these two basic lens models. We plot the magnitude and phase of the magnification/amplification factor. All the relevant mathematical and theoretical frameworks attached to the wave optics of these two gravitational lens models are discussed in this study. Furthermore, we apply one of these lens models (eg., the point mass lens model) to a simulated sine gaussian signal and a modelled gravitational wave signal from binary black hole merger system and estimate the lensing and signal parameters using nested sampling algorithm. We repeat the same study in wave optics and geometric optics limit approximation.

The point mass lens model assumes compact objects with high density like black holes as the gravitational lens object. This is the most basic model of lens in gravitational lensing process. The singular isothermal sphere (SIS) lens is the model which assumes cold dark matter halos in galaxies, clusters of galaxies and/or stars as its lens object. Both the lens models assume different properties and follow different lensing effects in wave optics and geometric optics approximation. They are studied in detail throughout this research.

1.3 Wave Optics and Geometric Optics limit

Gravitational lensing effects predominantly depends on two main lensing parameters:

- a. The mass of the gravitational lens object (referred to as M or M_L in the remainder of the study)
- b. The wavelength of the radiation (referred to as λ in the remainder of the study)

The lens mass M_L is in units of distance here, because it is multiplied by a factor (G/c^2) , which is the ratio of the gravitational constant and the square of the speed of light. If the wavelength of the radiation due to the propagation of gravitational wave λ is much greater than the lens mass (which is scaled to the unit of distance), $M \ll \lambda$, we can clearly say that the lensing could be appropriately described using wave optics limit approximation. If the wavelength is much smaller than the lens mass scale, then the lensed wave will behave in geometric optics limit approximation as described by the famous Fermat's principle. (T. R. 2006)

Wave optics deals with a mathematical integral called diffraction integral which will in turn represent the amplification in the amplitude of a wave that is magnified by lensing. Conventionally, gravitational lensing of light from astrophysical objects were treated only in the geometric optics limit because the wavelength of the light from those massive sources were typically smaller than the mass (distance-scaled) of the astrophysical objects under study. But when we focus on gravitational lensing of gravitational waves, the wavelength becomes huge wherein geometric optics limit no longer becomes a valid approximation because the diffraction effect comes into play. This research will focus both on cases where geometric optics limit comes into play and wave optics limit becomes valid, so that the gravitational lensing of gravitational waves could be studied for various mass ranges.

1.4 Organization of the scientific report

This scientific report is structured and organized as follows:

In this work, § 2 presents a theoretical framework of wave optics limit in gravitational lensing using thin lens approximation and geometric optics limit approximation for the two lens models under study. The lens equation for point mass lens model and singular isothermal sphere lens model is derived in the upcoming sections which determines the amplification produced by the particular lens model that varies with different source offset position and dimensionless frequencies in both geometric and wave optics limit. Several plots and figures explaining the oscillations produced by the lens equation is also presented. Transition between wave and geometric optics limit is also discussed in the same section.

Furthermore, § 3 explains the computational tools, statistical and numerical methods involved in the remainder of the study. It explains how nested sampling algorithm can be used in estimating several lensing and gravitational wave parameters involved in the lensing phenomena. A summary of how bilby is used as a major platform in producing source signals and recovering them is briefed in the same section. Generating GW signals using LALSuite python package is summarized in a sub-section. Basics of parameter estimation including defining likelihood, priors and using the interferometers in bilby is summarized as a sub-section in section 3.

In § 4, a sine gaussian source signal is modelled and several different properties of the signal is discussed and elaborated. Lensing parameters from point mass lens model is inserted into this sine gaussian model and the lensed signal is recovered estimating both the lensing and source signal parameters. Several results and analysis are presented in the

following section. As a sub-section, a binary black hole merger signal is simulated and modelled with different set of intrinsic and extrinsic parameters. This signal is then passed with point mass lens model parameters and a gravitationally lensed waveform is obtained. Nested sampling is done on the lensed signal and several lensing and gravitational wave parameters are estimated.

The results from modelled lensed sine gaussian and lensed binary black hole merger signal is produced in § 5. Several interpretations based on varying each parameter is briefed in the same section. Analyzing the black hole parameters from a lensed waveform while recovering them as they were not lensed help us determine the offset in parameter estimation if the signal was lensed but our recovery methods don't include lensing parameters in the estimation. These analysis and further discussion on them are summarized in § 5. The summary about strongly lensed and weakly lensed signals is discussed. The results are discussed both in wave optics and geometric optics limit and a smooth transition point between the two limits is also discussed in the results and analysis section.

A summary of all the results in existing literature and the novel analysis in this work is presented in § 6. The same section sets the conclusion for this work, scope of this work and possible future works and extension for this study. References are adhered in alphabetical order after the summary chapter. Appendix A presents the derivation maximum value of amplification factor for point mass lens model. Appendix B presents the derivation maximum value of amplification factor for SIS lens model. Appendix C presents a summary about the real-world equivalent of the source position parameter.

Chapter 2

Theoretical Framework

2.1 Wave Optics in Gravitational Lensing

In this sub-section, we briefly summarize the wave optics limit in gravitational lensing. (Schneider 1992, Luo 2015) We need a metric to represent the gravitational waves that propagates under the potential of a gravitational lens object. The metric is given as follows:

$$ds^2 = -1(1 + 2U)dt^2 + (1 - 2U)dr^2 \equiv g_{\mu\nu}^{(B)} dx^\mu dx^\nu \quad (2.1)$$

where $U(\mathbf{r})$ at any position vector \mathbf{r} is the gravitational potential of the massive and compact object that can act as the gravitational lens. Here $\mathbf{r} = (r, \theta, \phi)$ is the corresponding spherical coordinates. This $U(\mathbf{r})$ value is much lesser than unity ($\ll 1$). The background metric tensor can be represented and related to the linear perturbation of the gravitational wave as follows:

$$g_{\mu\nu} = g_{\mu\nu}^{(B)} + h_{\mu\nu} \quad (2.2)$$

It is practical to say that the gravitational wave under study will interact only with a limited region of space around the lens object when compared to large scale of distances between the source, lens and observer in all combinations. According to transverse-traceless Lorentz gauge condition (Einstein 1915) where $h_{\mu\nu}^{\nu} = 0$ and $h_{\mu}^{\mu} = 0$, we can say that,

$$h_{\mu\nu;\alpha}^{\alpha} + 2R_{\alpha\mu\nu\beta}^{(B)} h^{\alpha\beta} = 0 \quad (2.3)$$

Here the semicolon (;) operator is the covariant derivative with respect to the background metric tensor and the second term is twice the background Riemann tensor. When the wavelength of the radiation is smaller than the curvature radius of the background space-time, then the first term in (2.3) becomes zero.

By using the Eikonal approximation, a gravitational wave can be expressed in terms of the linear perturbation as follows:

$$h_{\mu\nu} = \phi e_{\mu\nu} \quad (2.4)$$

where $e_{\mu\nu}$ is the polarization tensor of the gravitational wave while ϕ is the scalar field. In gravitational lensing, we consider the polarization tensor as a constant because the change in the tensor is very small in our observation scenarios. Hence, the gravitational wave can be treated as a scalar wave represented by ϕ .

Considering the gravitational wave as a monochromatic wave travelling from a point source, we can represent its complex amplitude using the solution to the Klein-Gordon equation for curved spacetimes. (Asenio 2017)

$$\phi(\mathbf{r}, t) = \frac{A}{|\mathbf{r}|} F(\mathbf{r}) e^{-i(\omega t - \mathbf{k} \cdot \mathbf{r})} \quad (2.5)$$

where A is a constant of proportionality, $F(\mathbf{r})$ is the amplification factor due to lensing, $\omega = 2\pi f$ is the natural angular frequency of the GW, f is the normal frequency of the wave while \mathbf{k} is the vector that represents the wave number.

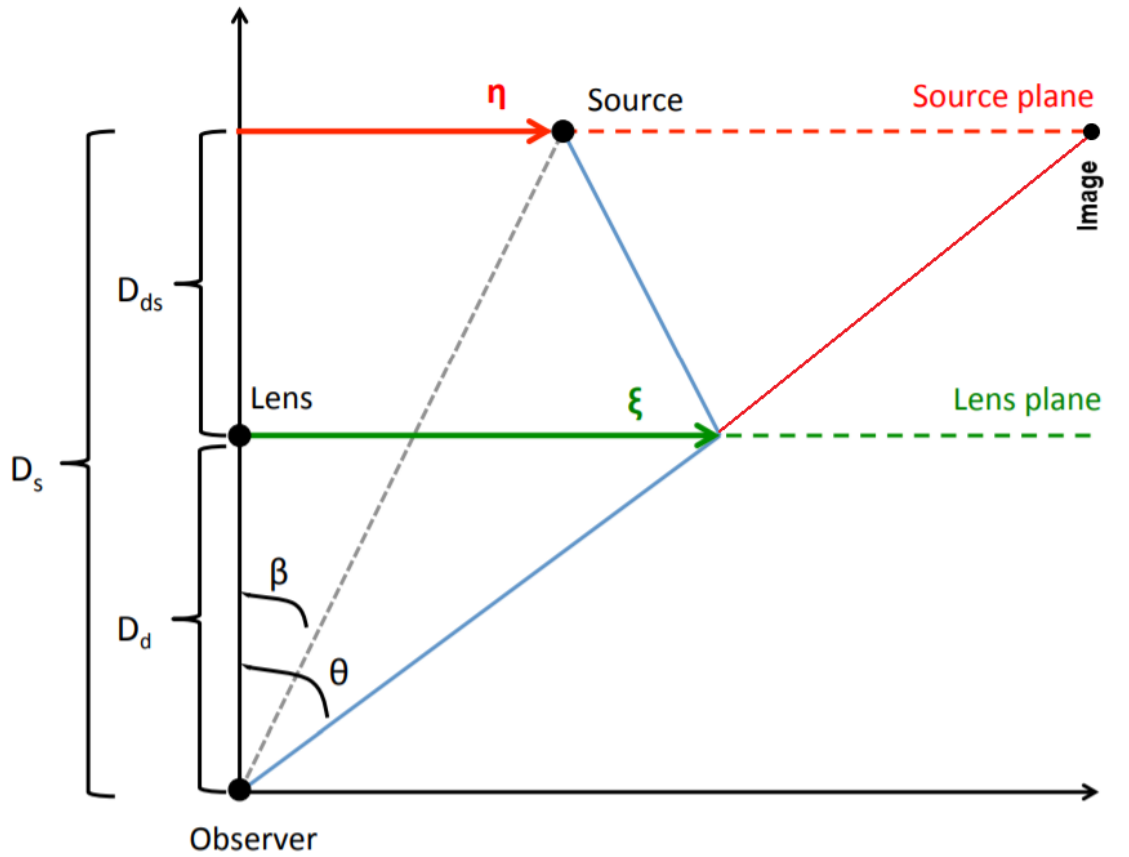


Figure 2.1: Gravitational lens geometry for the gravitational wave source (vectors shown in red), gravitational lens object (vectors shown in green) and the observer (ground or space-based interferometers). Path of gravitationally lensed signal is shown in blue and the sky position from where we obtain the GW image* on the source plane is shown in the maroon line. This interpretation is based on thin lens approximation (Matsunaga 2006). The angles shown here are vastly magnified compared to reality.

It is fair to write the amplification factor due to lensing as,

$$F(f) = \frac{\widetilde{\phi}^L(f)}{\widetilde{\phi}(f)} \quad (2.6)$$

*Note: When we refer to images obtained from gravitational lensing of GW in any part of this study, we mean the sound signal from the GW from a different sky position on the source plane than the original source position because in case of GW, we do not obtain any images.

where $\tilde{\phi}^L(f)$ is the lensed wave amplitude of the GW and $\tilde{\phi}(f)$ is the unlensed gravitational wave amplitude when gravitational potential, $U=0$. In Figure 2.1, the configuration of gravitational lensing phenomenon for a source, lens and observer separated by the distances D_{ds} , D_d and D_s respectively is shown. η is the source offset vector (a position vector) that represents the position vector of the massive gravitational wave source in the source plane. ξ is the impact parameter (a position vector) that is configured to the lens plane. This parameter is related to the Einstein angle using the relation $\xi_o = \theta_E D_d$ where θ_E (or simply Θ , as in Figure 2.1) is the Einstein angle. Here, we use thin lens approximation wherein the lens object is represented by its surface mass density $\Sigma(\xi)$ and based on the assumption that the gravitational waves are scattered over a lens plane of thin thickness. Further, using mathematical formulas and relations described in the scientific literature (Abramowitz & Stegun 1972, Matsunaga 2006), the amplification factor $F(f)$ at the interferometer can be described as follows:

$$F(f) = \frac{D_s \xi_o^2}{D_d D_{ds}} \frac{f}{i} \int d^2 \mathbf{x} \exp\{2\pi i f t_d(\mathbf{x}, \mathbf{y})\} \quad (2.7)$$

where $\mathbf{x}=\xi/\xi_o$ and $\mathbf{y}=\eta D_d/\xi_o D_s$ is the scaled versions of η and ξ and are dimensionless. T_d is the time of arrival of the gravitational wave at the observer from the source after lensing. The value of F is normalized at $U=0$ which is equivalent to a scenario where the limit tends to no lens and thus $|F|=1$. The time delay function is described as follows:

$$t_d(\mathbf{x}, \mathbf{y}) = \frac{1}{2} |\mathbf{x} - \mathbf{y}|^2 - \psi(\mathbf{x}) + \phi_m(\mathbf{y}) \quad (2.8)$$

Here, $\psi(\mathbf{x}) = \int_{-\infty}^{\infty} dz U$ is the gravitational potential integrated over two-dimensional space. We know that, due to lensing, the two images will have a certain time difference in reaching the observer which is described by the time delay function as described above. The integral in equation (2.7) integrates over all possible paths and the two images represent the time delay between different possible paths (through the lens plane) that the wave could take. The function ϕ_m that depends on the source position is inserted into this equation to set the minimum time delay between these images to zero value. If we assume the lens model to be symmetric, then we get the following generalization case for the amplification factor of the GW that is lensed,

$$F_w(w, y) = -w \exp\left(\frac{1}{2} w y^2\right) \int_0^{\infty} x J_0(wxy) \exp\left\{i w \left[\frac{1}{2} x^2 - \psi(x) + \phi_m(y)\right]\right\} dx \quad (2.9)$$

where $J_0(wxy)$ is the Bessel function of first order which depends on the product of w , x and y . In this final equation, we assume that the gravitational potential will depend only on \mathbf{x} which is equivalent to the absolute value of x . Similarly, the ϕ_m function depends only on \mathbf{y} which is equivalent to the magnitude of y . In the above mentioned equation, the important parameter w is the dimensionless frequency parameter which is equal to $8\pi M_L f$ where M_L (L subscript stand for the lens) is the redshift mass of the lens object that is equal to $(1+z_L)M$. In this study, we predominantly consider $z_L=0$ for galactic and other compact object sources that are nearby making $M_L \sim M$. We can clearly notice that w is directly proportional to the

ratio of lens mass and wavelength of the radiation (M_L/λ). Thus, this quantity w is that lensing parameter which describes which type of optics limit is applicable to the lensing process of the gravitational wave under study: wave optics or geometric optics limit. Hence, the amplification factor due to gravitational lensing is heavily dependent on the dimensionless frequency w and source offset factor y .

2.1.1 Geometric Optics Approximation

In this sub-section, we will brief about small wavelength limit in the wave optics wherein $w \gg 1$ which will approximate to conventional geometric optics limit evaluation in gravitational lensing phenomena. In this limit, frequency of the GW radiation is extremely higher than the inverse of the time delay between lensed and unlensed images i.e., $f \gg t_d^{-1}$. According to the Fermat's principle, the stationary points on the time delay function $t_d(\mathbf{x}, \mathbf{y})$ contributes to the integral in the final wave optics equation. This renders the following amplification factor equation in the geometric optics limit.

$$F_g(w, y) = \sum_j |\mu(x_j)|^{\frac{1}{2}} \exp\left(iwt_d(x_j, y) - i\frac{n_j}{2}\pi\right) \quad (2.10)$$

where the magnification of any arbitrary j -th image is $\mu(x_j) = 1/\det(\partial y/\partial x_j)$ and $n_j = 0, 1, 2, \dots$. For the case of lensing through multiple images in the geometric optics limit, the summation in this final expression means that the observed lensed GW is represented by the superposition of several waves with amplitude described by the factor $|\mu(x_j)|^{1/2}$ and phase expressed as $wt_d(x_j, y) - n_j\pi/2$.

2.2 Point Mass Lens

When the massive lens object that takes its position in-between the GW source and the observer is a black hole or a compact isolated star within a galaxy, then its mass distribution is point-like and it can be regarded as a point mass gravitational lens model.

In general, the deflection potential of the GW is given by

$$\psi(\mathbf{x}) = 4G \frac{D_d D_{ds}}{D_s} \int_{-\infty}^{\infty} d^2\Sigma(s) \log|\mathbf{x} - \mathbf{s}| \quad (2.11)$$

where the surface mass density for any mass model in lens plane is given by

$$\Sigma(\mathbf{x}) = \int_{-\infty}^{\infty} dz \rho(\mathbf{x}, z) \quad (2.12)$$

Where $\rho(\mathbf{x}, z)$ is the mass density profile of the lens model under consideration which is directly related to the Newtonian potential as $\nabla^2 U = 4\pi G\rho$. This is a mathematical proof that the amplification factor for any lens model depends on mass density distribution and gravitational deflection potential.

The surface mass density for such a point-mass distribution of matter is $\Sigma(\mathbf{x}) = M\delta^{(2)}(\xi)$. For

point mass lens model, we write $\rho(\mathbf{x},z) = M\delta^{(2)}(\boldsymbol{\xi})\delta^{(1)}(z)$ where M is the mass of the lens object described by the point mass distribution model. For such mass distributions, the Einstein angle can be described as follows:

$$\theta_E = \sqrt{\frac{4GM D_{ds}}{D_d D_s}} \approx 3 \times 10^{-6} \left(\frac{M}{M_\odot}\right)^{\frac{1}{2}} \left(\frac{D_d D_s}{1 \text{ Gpc}}\right)^{-\frac{1}{2}} \text{ arcsec} \quad (2.13)$$

Gravitational deflection potential for this mass distribution model is given by $\psi(x) = \log x$. Substituting all these expressions on the analytical formula for amplification factor of any gravitational lens model of lensing phenomena in a GW radiation gives us the following lens equation for the point mass lens model:

$$F_w(w, y) = \exp\left[\frac{i}{2}w(y^2 + \log\left(\frac{w}{2}\right))\right] \exp\left(\frac{\pi}{4}w\right) \Gamma\left(1 - \frac{i}{2}w\right) {}_1F_1\left(1 - \frac{i}{2}w, 1; -\frac{i}{2}wy^2\right) \quad (2.14)$$

where ${}_1F_1(a,b;c)$ is the confluent hypergeometric function of the first kind. Also known as Kummer's function which is in turn a solution of Kummer's differential equation. Bessel equations can be easily solved using hypergeometric functions and thus, the generic lens equation, after solving for point mass lens model yields a function with confluent hypergeometric function. (Magnus 1996) We know that, Γ is the gamma function which extends from normal factorials to complex numbers except non-positive integers. The maximum magnification of source image can be achieved when the source is in line with the observer i.e., when the source offset factor $y=0$. The above-mentioned equation can be solved for $y=0$, which after mathematical and analytical evaluations yield

$$F_{max}(w, y = 0) = \sqrt{\frac{\pi w}{1 - \exp(-\pi w)}} \quad (2.15)$$

When we consider the approximation based on geometric optics limit, the point mass lens model will consist of two images in this limit. Solution to equation (2.15) in Appendix A. Thus, the lens equation will yield the following solutions:

$$F_g(w, y) = |\mu_+|^{1/2} - i|\mu_-|^{1/2} \exp\left\{iw \left[\frac{y\sqrt{y^2+4}}{2} + \ln\left(\frac{\sqrt{y^2+4}+y}{\sqrt{y^2+4}-y}\right) \right]\right\} \quad (2.16)$$

where amplification of each of the two images (GW sound signal) is given by

$$\mu_{\pm} = \frac{1}{2} \pm \frac{y^2 + 2}{2y\sqrt{y^2 + 4}} \quad (2.17)$$

From the solution to the classical lens equation, $\mathbf{x} + \mathbf{y} - \nabla\psi(\mathbf{x})=0$, we can say that we obtain image position $\mathbf{x}_{\pm} = \mathbf{y}/2 + \sqrt{\mathbf{y}^2 + 4}/2$. Thus, we get two images in all these cases.

2.3 Singular Isothermal Sphere Lens

Modelling a cold dark matter halo can be done by studying the second model under this research: singular isothermal sphere (SIS) lens model.

The density profile for the case of singular isothermal sphere is described as

$$\rho(x, z) = \frac{\sigma_v^2}{2\pi G(|\xi_o x|^2 + z^2)} \quad (2.18)$$

where σ_v is the dispersion velocity described by the singular isothermal sphere mass distribution. The surface mass density for the SIS model is defined as

$$\Sigma(x) = \frac{\sigma_v^2}{2G\xi_o x} \quad (2.19)$$

While the gravitational deflection potential $\psi(x)$ is equal to x . All the equations enable us to deduce the Einstein angle for the SIS lens model. This is given by

$$\theta_E = 4\pi\sigma_v^2 \frac{D_{ds}}{D_s} \approx 3 \times 10^{-5} \left(\frac{\sigma_v}{1 \frac{\text{km}}{\text{s}}} \right)^2 \left(\frac{D_{ds}}{D_s} \right) \text{arcsec} \quad (2.20)$$

Substituting all these expressions on the analytical formula for amplification factor of any gravitational lens model of lensing phenomena in a GW radiation gives us the following lens equation for the SIS lens model:

$$F_w(w, y) = \exp\left[\frac{i}{2}wy^2\right] \sum_{n=0}^{\infty} \left\{ 2w \exp\left(i\frac{3\pi}{2}\right) \right\}^{\frac{n}{2}} \frac{\Gamma\left(1 + \frac{n}{2}\right)}{n!} {}_1F_1\left(1 + \frac{n}{2}, 1; -\frac{i}{2}wy^2\right) \quad (2.21)$$

The maximum amplification that can be achieved by gravitational lensing of gravitational waves when the lens object is described by a SIS mass distribution model will be obtained by solving this equation for a source offset value of zero, i.e., $y=0$. This gives

$$F_{max}(w, y = 0) = \left| 1 + \frac{1}{2}(1 - i) \exp\left(-\frac{1}{2}w\right) \sqrt{\pi w} \left[1 + \text{Erf}\left(\frac{\sqrt{w}}{2}(1 - i)\right) \right] \right| \quad (2.22)$$

where Erf is a complex function of the complex variable under parenthesis, commonly known as error function. Derivation of equation (2.22) in Appendix B.

As the final mathematical analysis of this sub-section, let us consider the magnification/amplification factor of SIS lens model in the regime of geometric optics limit approximation. For the case of an SIS lens model, two images are formed for $y < 1$ at minimum and saddle points while one stationary image point is formed for $y \geq 1$. This can be described by the following piece-wise defined function.

$$F_g(w, y) = \begin{cases} |\mu_+|^{1/2} - i|\mu_-|^{1/2} \exp\{i2wy\} & \nabla y \leq 1 \\ |\mu_+|^{1/2} & \nabla y \geq 1 \end{cases} \quad (2.23)$$

where amplification of each of the two image is given by

$$\mu_{\pm} = \pm 1 + \frac{1}{y} \quad (2.24)$$

As we see from the final equation, for y values less than 1, double images are formed while for y greater than 1, only one image is formed in the geometric optics limit regime. This SIS lens model is quite efficient as it can be used to describe more realistic astrophysical lens objects such as galaxies, halos and star clusters.

Lens Model	$\phi_m(y)$	w Dimensionless Frequency
Point Mass	$(x_m - y)^2/2$	$8\pi Mf$
Singular Isothermal Sphere	$y+1/2$	$2\pi f(4\pi\sigma_v^2)^2 (D_d D_{ds}/D_s)$

Table 2.1: Comparison of lensing parameters for Point-mass and Singular Isothermal Sphere

A tabulation of the values of $\phi_m(y)$ that makes the minimum time delay function round to zero and the value of dimensionless frequency for both the lens models is summarized in Table 2.1. These values have been used while computing the magnitude and phase of the amplification factor in the upcoming sections.

2.4 Magnitude of the Amplification Factor

From the analytic wave equation that we have derived for point mass lens model (2.14) and singular isothermal sphere lens model (2.21), we can plot the magnitude or absolute value of the amplification factor as a function of the characteristic gravitational wave radiation parameter w which is also called the dimensionless frequency as it is proportional product of lens mass (scaled to time – multiplied by a factor of G/c^3) and frequency of the GW radiation. Figure 2.2 shows the magnitude of amplification factor plotted against the dimensionless frequency for a constant value of source offset position y . The same curve is plotted for three other values of y . The source position is fixed as 0.1, 0.25, 0.5 and 1.0.

For $w \geq 1$, i.e., when the dimensionless frequency is greater than unity, severe oscillation is observed in the absolute value of amplification factor due to lensing of the gravitational wave. This oscillation occurs as a result of interference in the waves formed between the multiple images due to gravitational lensing as described by the wave optics approximation.

The amplitude of such oscillatory behavior in the amplification factor for varying w that is greater than 1 decrease with increasing value of y from 0.1 to 1.0 which can also be observed in the Figure 2.2.

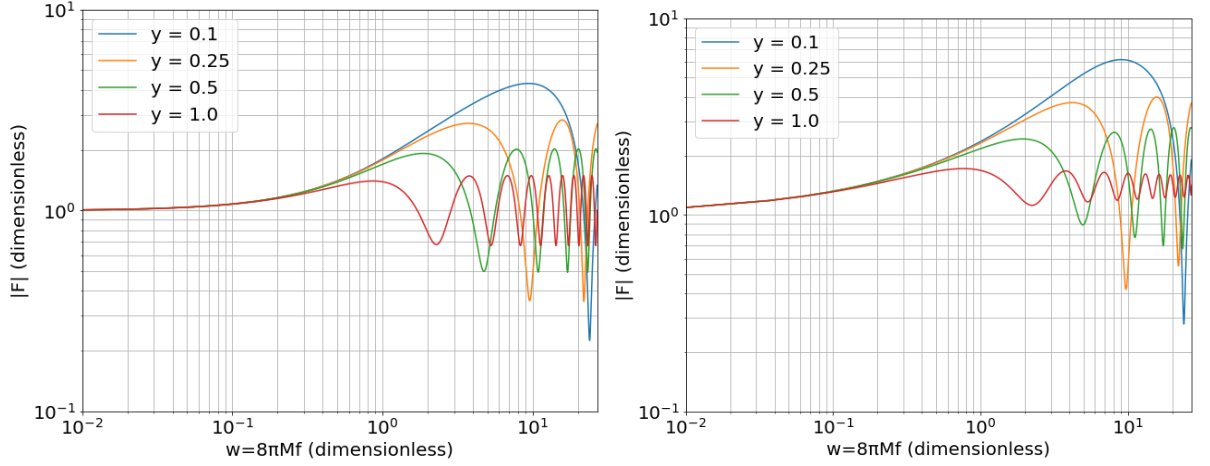


Figure 2.2: Magnitude of the amplification factor of point mass lens model (**Left**) and singular isothermal sphere lens model (**Right**) with respect to varying values of dimensionless frequency ($w=8\pi M_L f$) for a specific source offset value (i.e., $y=0.1, 0.25, 0.5, 1.0$)

For $w \leq 1$, i.e., when the dimensionless frequency is lesser than unity, the magnitude of amplification is very small. This can be explained as a consequence of the diffraction effect that we discussed earlier. The amplification is less because when w is smaller than unity, the wavelength is very large and thus the incoming gravitational wave does not feel the existence of the intervening lens object along its path to the observer. When w increases to a value greater than 1.0, then the $F(w, y = \text{constant})$ curve slowly converges to geometric optics limit.

The highest magnitude of amplification factor occurs when $y=0.1$ and $w \approx 10$ wherein $|F(w, y)| \approx 3.2$, i.e., when the source offset is quite low and dimensionless frequency is ten times unity, we obtain high magnification of the GW source signal that is three times amplified for point mass lens model.

Figure 2.3 shows the magnitude of amplification factor plotted against the source offset position y for a constant value of dimensionless frequency w . The same curve is plotted for two other values of w . The dimensionless frequency is fixed as 20, 5 and 1.

This plot proves that the oscillatory behavior increases for increasing values of dimensionless frequency w (from 1 to 20). When the source position y gets closer to zero, that is, when the source gets aligned with the gravitational lens object, the amplification factor tends to increase and converge at one point for $y=0$ that is described by the equation we derived in the previous sub-sections. Given that the dimensionless frequency is directly proportional to the frequency of the gravitational wave under study taking the lens mass scale to be a constant value, we can say that, as the frequency of the source signal increases oscillatory behavior of $F(w = \text{constant}, y)$ function due to interference of lens

images comes into play.

In the same plot, it is also visible that, when the source position y becomes greater than unity, damped oscillatory behavior of $F(w=\text{constant},y)$ appears because the wave starts to behave in accordance with the geometric optics limit wherein only a single image exists for source position $y \geq 1.0$.

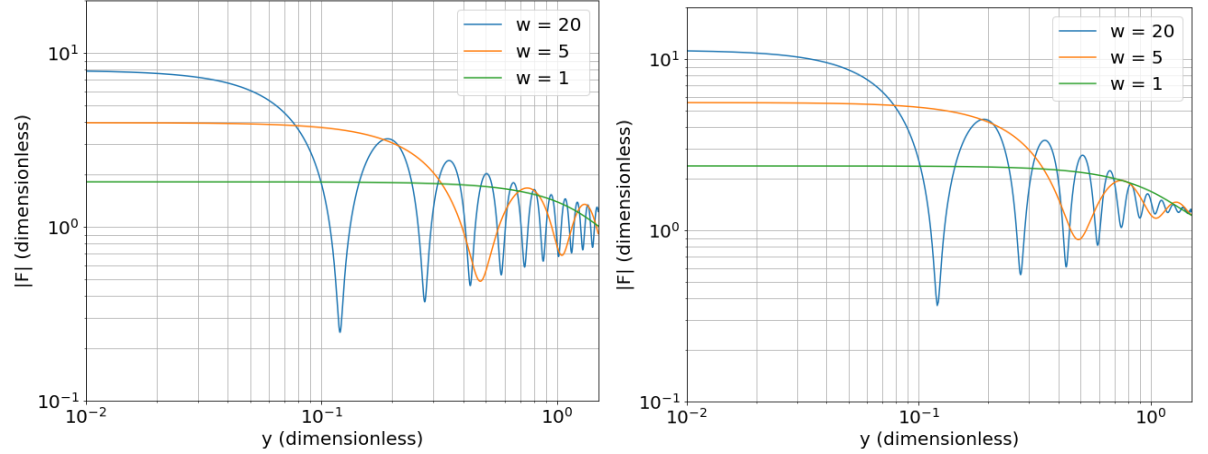


Figure 2.3: Magnitude of the amplification factor of point mass lens model (**Left**) and singular isothermal sphere lens model (**Right**) with respect to varying values of source offset for specific values of dimensionless frequency ($w=8\pi M_L f$) (i.e., $w=1, 5, 20$)

Another interesting fact to notice is that, the highest magnitude of amplification factor occurs when $y=0.1$ and $w \approx 10$ wherein $|F(w,y)| \approx 5.0$, i.e., when the source offset is quite low and dimensionless frequency is ten times unity, we obtain high magnification of the GW source signal that is five times amplified for singular isothermal sphere lens model. This magnification value is higher than the one we obtain due to point mass lens model whereas we expect this to be vice-versa as the point-mass like lens objects are denser and compact. This is a theoretical verification that singular isothermal sphere lens produces higher magnitudes of amplification when compared to point mass lens model. In both the lens models, when $y < 1$, we see two stationary image points at the minimum and saddle points whereas when $y \geq 1$, we see only one image at one stationary point. This is heavily visible at higher values of dimensionless frequency because that is when the wave optics also agrees with geometric optics approximation and both the scenarios produce same amount of magnification.

2.5 Phase of the Amplification Factor

From the analytic wave equation that we have derived for point mass lens model and singular isothermal sphere lens model, we can plot the phase of the amplification factor as a function of the characteristic gravitational wave radiation parameter w using the following relation:

$$\theta_{F(wave)}(w, y) = -i \ln \left[\frac{F(w, y)}{|F(w, y)|} \right] \quad (2.25)$$

When the dimensionless frequency w is greater than unity, $\Theta_F(w, \gamma)$ starts to approximately converge with the phase defined by geometric optics limit approximation. This can be described by the following equation:

$$\theta_{F(geo)}(f) = \arctan \left[\frac{-|\mu_-|^{\frac{1}{2}} \cos(2\pi f \Delta t_d)}{|\mu_+|^{\frac{1}{2}} + |\mu_-|^{\frac{1}{2}} \sin(2\pi f \Delta t_d)} \right] \quad (2.26)$$

where $|\mu_-| = 0$ when γ is greater than unity for the singular isothermal sphere model. On analyzing the above equation, we can say that the phase of the amplification factor oscillates between $-\arctan[|\mu_-|^{1/2} / |\mu_+|^{1/2}]$ and $\arctan[|\mu_-|^{1/2} / |\mu_+|^{1/2}]$ with a time period of $2\pi f \Delta t_d$ wherein the typical time delay is $\Delta t_d = 4M_L$.

Figure 2.4 shows the phase of amplification factor plotted against the dimensionless frequency for a constant value of source offset position γ . The same curve is plotted for three other values of γ . The source position is fixed as 0.1, 0.25, 0.5 and 1.0.

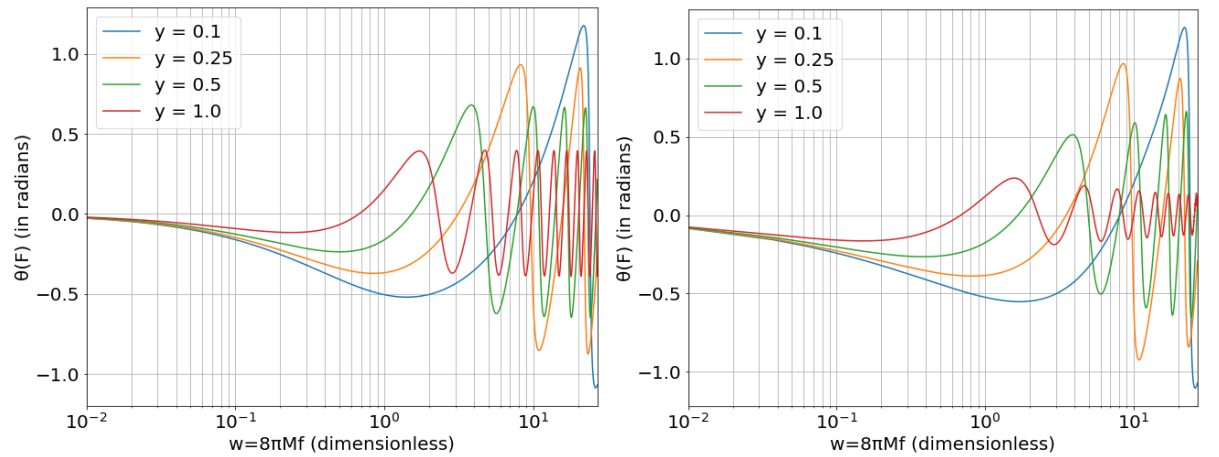


Figure 2.4: Phase of the amplification factor ($\Theta_F(w) = -i \ln[F(w)/|F(w)|]$) of point mass lens model (**Left**) and singular isothermal sphere lens model (**Right**) with respect to varying values of dimensionless frequency ($w=8\pi M_L f$) for a specific source offset values (i.e., $\gamma=0.1, 0.25, 0.5, 1.0$)

The behavior of the phase is very similar to that of the magnitude of the amplification factor. The oscillatory wave behavior appears in both phase and magnitude of the magnification factor due to the two lens models under study in this research. We can see that, as the dimensionless frequency increases, the phase of the lensed waveform starts to obey geometric optics limit approximation.

Figure 2.5 shows the phase of amplification factor plotted against the source offset position γ for a constant value of dimensionless frequency w . The same curve is plotted for two other values of w . The dimensionless frequency is fixed as 20, 5 and 1.

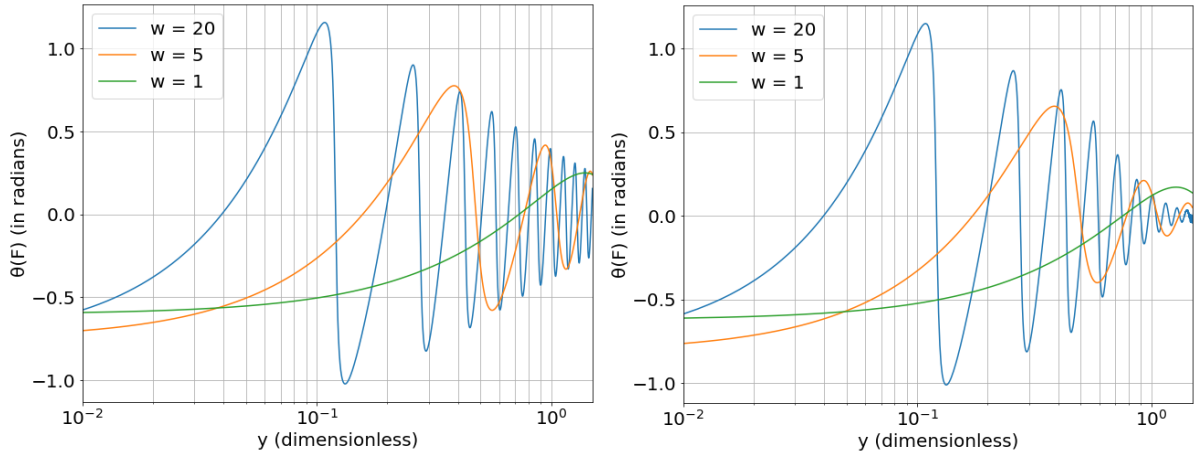


Figure 2.5: Phase of the amplification factor ($\Theta_F(w) = -i \ln[F(w)/|F(w)|]$) of point mass lens model (**Left**) and singular isothermal sphere lens model (**Right**) with respect to varying values of source offset for specific values of dimensionless frequency ($w=8\pi M_l f$) (i.e., $w=1, 5, 20$)

From this plot, we can conclude that as the source offset position y increases, the ratio of μ_- and μ_+ decreases and thus, the amplitude and phase of the oscillatory behavior in the amplification factor ultimately decreases.

2.6 Transition between geometric and wave optics limit

In theory, we have already proved that wave optics limit holds good for lower values of dimensionless frequency w creating diffraction effects and geometric optics limit holds true for higher values of w creating interference effects. Since we deal with different lens mass and sampling frequency and both these values are directly proportional to the dimensionless frequency w , in real-time scenarios, both wave optics and geometric optics limit approximation should be used in the source signal to study the effects of gravitational lensing on gravitational waves to its proper potential.

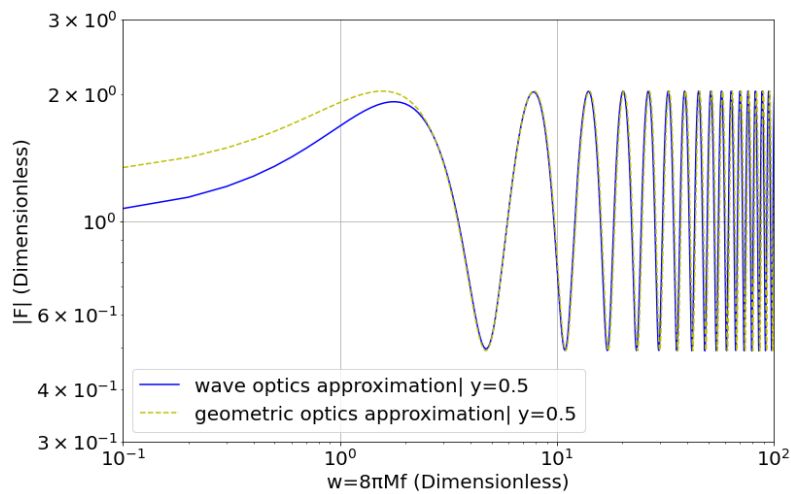


Figure 2.6: Transition between wave optics and geometric optics approximation for $y=0.5$ at higher values of dimensionless frequency i.e., $w \gg 1$. This argument hold for various other values of y as well

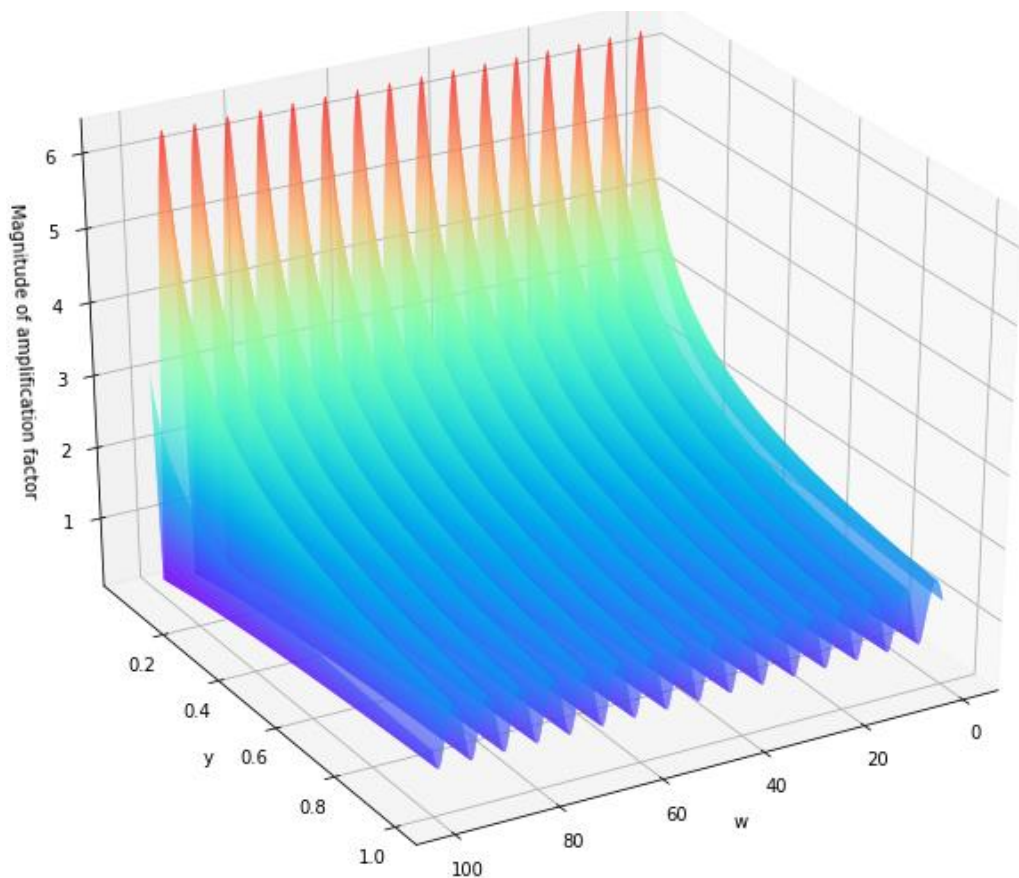
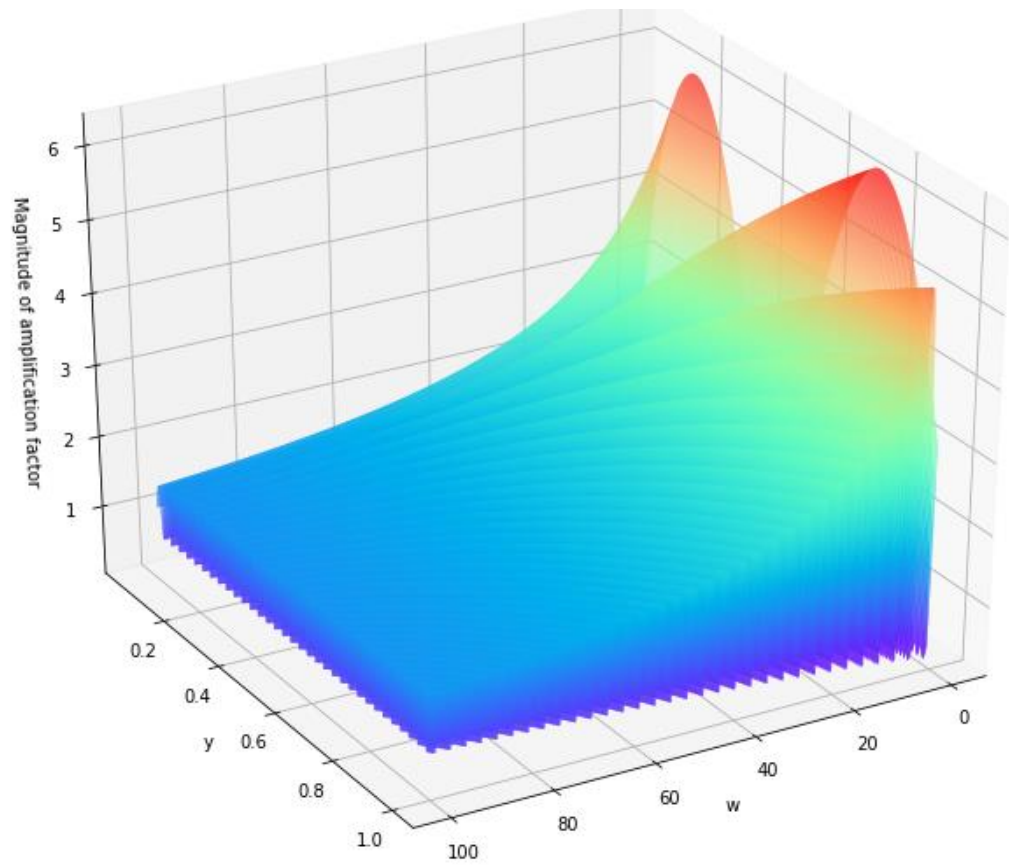


Figure 2.7: 3D surface plots of $|F_w(w,y)|$ (Left) and $|F_{geo}(w,y)|$ (Right) (both are dimensionless) as a function of dimensionless frequency and source position (dimensionless). Note that the plots are not scaled to logarithmic scale

In Figure 2.6, the resultant lens equation from both the limits is plotted (solid lines – wave optics limit, dashed lines – geometric optics limit), to find that value of w wherein the transition between the two limits happen unnoticeably. It is clear that for the values of w greater than unity, both the limits start to agree with the same absolute values of magnification factor. In this range, we choose an optimal value, say $w=10$. This value of w is chosen as the transition point between the two limits. Two different lens equation functions are defined and depending on the value of w , one of those function gets called and in the end an array of amplification factor values is created by joining appropriate values from the two limits. By this way, we can accommodate several different range of lens mass values for the compact point-mass like lens object. The entire analysis for BBH merger signal has been performed by using both the wave optics and geometric optics limit transitioning between these two limits depending on the w value.

Three-dimensional surface plots for the co-ordinates w , y , $F(w,y)$ and resulting 3D plot is shown in Figure 2.7. This plots also reapproves that both the limits agree on the same values for higher values of dimensionless frequency w . However, it is also important to note that, geometric optics limit on lower values of w gives wrong values while wave optics approximation on very high values of w is not defined.

Chapter 3

Statistical and Computational Methods

3.1 Bayesian methods of parameter estimation

Bayesian inference is one of the mathematical methods which uses Bayes' Theorem to estimate the probability of a hypothesis given that enough evidence and information on the input variables is available. Bayesian methods are especially very useful and important in dynamic analysis of the input data sequence in a particular hypothesis. From early mathematics, we know that, Bayes' Theorem describes the probability of an event using the following relation:

$$P(x|\text{data}, M) = \frac{P(\text{data}|x, M)P(x|M)}{P(\text{data}|M)} \quad (3.1)$$

Bayes' Theorem has its major application on Bayesian Inference. Bayes' Theorem relates the degree of belief in a parameter before and after considering the amount of evidence available to the support the parameter. In the above equation (3.1), $P(x|M)$ is the prior or initial knowledge about the random variable x , $P(x|\text{data}, M)$ is the posterior on the parameter x after obtaining the information that the model M and data is valid and true, the term $P(\text{data}|x, M)$ is the likelihood and $P(\text{data}|M)$ is the evidence that the model M provides for the data.

This paradigm of parameter estimation follows modelling the distribution of known and unknown (random) variables, defining the prior distribution on those random variables and updating our posteriors based on the prior, likelihood and evidences.

3.1.1 Bayes Factor and Bayesian evidence

We use Bayes Factor as an alternate to classical frequentist hypothesis test. Bayes Factor helps in providing support for one statistical model over the other. Note that, Bayes factor or odds ratio does not say whether the model is true or not.

$$K = \frac{P(D|M_1)}{P(D|M_2)} \quad (3.2)$$

where $P(D|M_1)$ is the posterior for the data given that the model M_1 is true and $P(D|M_2)$ is the posterior for the data given that the model M_2 is true. If the Bayes Factor value is greater than 1, then model 1 is favored. If the Bayes Factor value is less than 1, then model 2 is favored.

Bayesian evidence acts as a normalization factor in parameter estimation problems. It is also

called marginal likelihood. The ratio of these evidences gives the Bayes Factor. In parameter estimation problems, evidence play a small role of normalization while in model selection problems, it plays a major role wherein ratio of evidences gives the Bayes Factor which in turn says which model is favorable.

3.2 Nested Sampling

In this research, we use a computational approach called nested sampling algorithm to the lensed waveform models for parameter estimation. This algorithm provides posterior samples and estimates of Bayesian evidence. This algorithm performs better than MCMC parameter estimation for multi-modal distributions because there is no need to specify any proposal density here.

Nested sampling plots posterior distribution by having a set of samples specified within the prior range called 'live points' and iteratively update them with a condition that the new samples should have a greater likelihood than the older ones. In standard nested sampling, the amount of shrink in the prior range remaining is the same in each step. We use dynamic nested sampling in this work. Here, we dynamically vary the number of live points in order to increase the accuracy of calculation for some posterior samples. This is very effective than standard nested sampling because in standard one, most of the computational execution time goes in estimating all the posterior samples with little weight that makes no contribution to the parameter estimation calculations. (Higson 2019)

3.2.1 Dynesty – Nested Sampling Algorithm

In this research, we use dynesty: a dynamic nested sampling algorithm (Speagle 2018) for estimating the posteriors and evidences, also known in Bayesian analysis as marginal likelihoods. Dynamic nested sampling takes the advantage of parameter estimation of posteriors like in the famous Markov Chain Monte Carlo methods (popularly referred as MCMC algorithm) along with focusing on the aims of nested sampling like estimating the evidences and producing samples in multi-dimensional distributions.

3.3 Bilby - Bayesian Inference Library

Bilby is a user-friendly Bayesian statistics library (Ashton 2019) that is widely used in the field of gravitational wave astrophysics because in GW astronomy, the signal and source' physical properties are estimated predominantly using Bayesian methods of parameter estimation. This python module provides an extremely convenient parameter estimation infrastructure that performs accurate sampling of input data in the recovery model.

This research uses Bilby along with Lalsuite (LALSimulation) and gwpy packages in Jupyter Notebook (Python) for modelling the source signal, adding lensing parameters to it and estimating the resulting parameters. One of the major advantage of using Bilby for our problem statement is that it allows adding interferometer noises to the modelled source signal and thus we will be able to simulate our results at a practical level of signal -to-noise-ratio and produce results that are closer to the ones we obtain from the observation runs of existing LIGO/VIRGO detectors.

Bilby is one of the best and robust interfaces to perform parameter estimation on several lensing and GW source parameters. Here, we access LIGO data using the GWPY module. Bilby also allows defining several different types of source functions, likelihood and priors along with prior constraints and plot corner plots generated from the samples produced using the nested sampling algorithm. In the next section, we will look in detail about the sampler that we use in this study.

3.4 LALSuite – LIGO gravitational wave analysis algorithm

LALSuite (stands for LIGO Scientific Collaboration (LSC) Algorithm Library Suite in gravity research) python package was initially designed to search for gravitational wave signal amidst the noises in the LIGO and VIRGO ground-based interferometers in each of its observing runs and characterize several different astronomical signals within the series of data from the interferometers in time-domain. This is an open source public domain package available for Linux and macOS. It supports run on Colab – Google Colaboratory – which allows writing and executing jupyter notebooks in browser windows with free access to its GPU card.

This research will use LALSuite for source-modelling binary black hole merger gravitational wave signals. (LSC 2018) This will enable simulating gravitational wave signals (Varma 2016) for a defined set of source parameters and sky positions based on LIGO and VIRGO existing observing run data stream. This package has a collection of data analysis interfaces with the LIGO collaboration which enables applying several different statistical methods on such data and deriving conclusions on the numerical properties and correlation between random variables present in the data.

LALSimulation is very useful in creating the gravitation waveforms as per the requirement in any scientific problem statement and generating real time noise waves along with the source data. Most of the modules especially the ones used in this research have straightforward syntax and are easy to interpret and implement.

Chapter 4

Source Signal

From this chapter, we will mainly focus on the gravitational lensing of gravitational wave events with the lens object having a mass distribution similar to point-mass like astrophysical objects such as black holes and compact stars in distant galaxies. We will consider model two different types of source signals in frequency domain, attach the lensing model to it and generate a lensed waveform which we later recover and estimate several different lensing and input signal parameters.

Firstly, we will generate a sine-gaussian source model in the frequency domain and in the second scenario, we will generate a gravitational wave signal from a binary black hole merger event.

4.1 Sine-Gaussian Signal

Firstly, a sine-gaussian signal in the frequency domain is defined outside the scope of Bilby for a particular frequency f_0 and amplitude A . A sine-gaussian signal is nothing but a normal sine wave signal modulated by a Gaussian wave envelope and its characteristic parameter is the central frequency of the signal. The function is declared in such a way that it returns a structure of plus and cross polarizations of sine-gaussian wave taking amplitude and frequency as the major arguments. The plus and cross polarizations of the function are defined as follows:

$$h_+^{SG}(f) = \frac{1}{2}A\sqrt{\pi}\tau \exp\left(-(\pi\tau(f - f_0))^2 + i\phi\right) \quad (4.1)$$

$$h_\times^{SG}(f) = h_+^{SG}(f) \exp\left(i\frac{\pi}{2}\right) \quad (4.2)$$

It is important to note that we define the sine-gaussian signal in frequency domain because our lens equation varies as a function of dimensionless frequency w which is directly proportional to the frequency of the source signal under study. Now, we use Bilby to model the sine-gaussian signal by injecting appropriate values for A , f_0 , τ and ϕ and defining the sine-gaussian function that returns plus and cross polarization as the frequency domain source model. This will generate a waveform that can further be passed on to the LIGO interferometers to create a simulated noise form to be added to the sine-gaussian signal.

The sine gaussian signal can then be lensed by multiplying the point mass lens model's amplification factor equation with the plus and cross polarization of the sine-gaussian signal as follows:

$$h_+^{SG \text{ lensed}}(f) = h_+^{SG}(f) \times F(w = 8\pi M_L f, y = 0.1) \quad (4.3)$$

$$h_\times^{SG \text{ lensed}}(f) = h_\times^{SG}(f) \times F(w = 8\pi M_L f, y = 0.1) \quad (4.4)$$

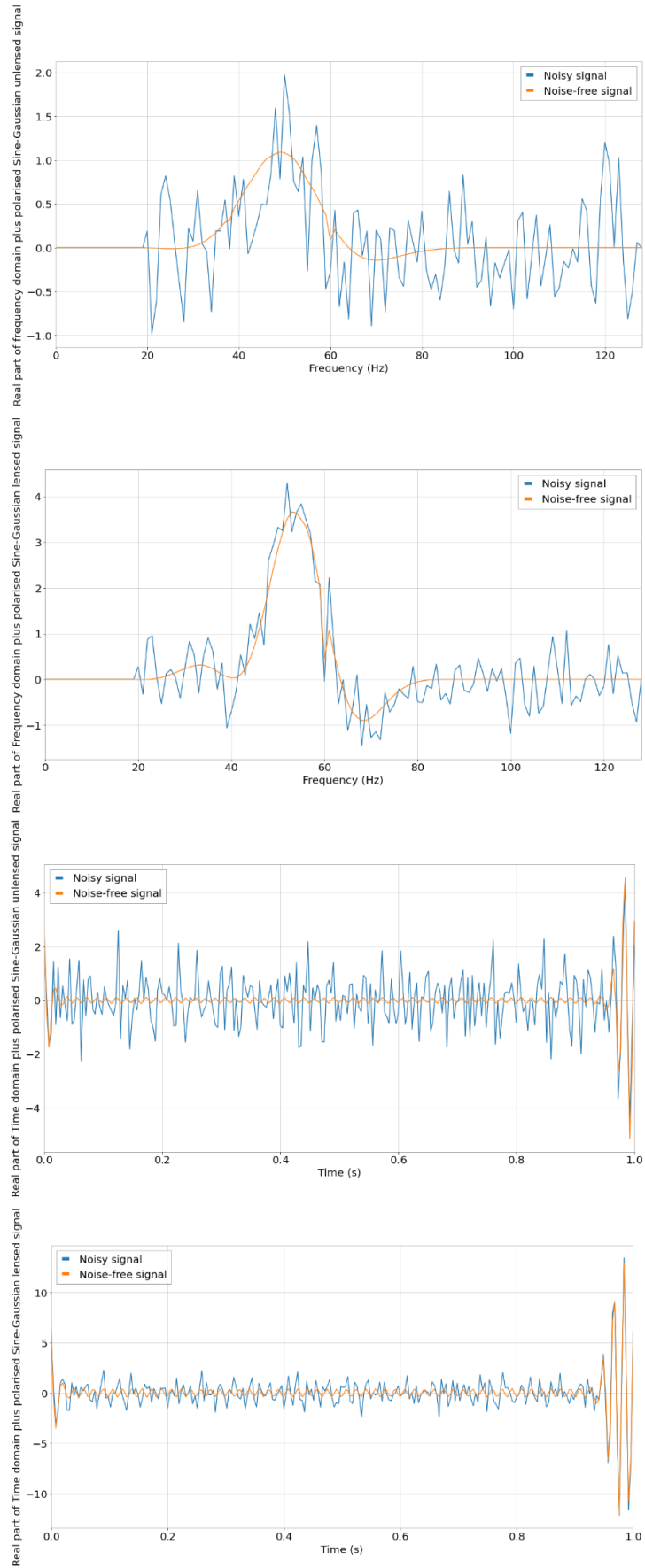


Figure 4.1: Frequency domain sine-gaussian unlensed signal at a frequency of $f_0=50\text{Hz}$ **(Top)**, Frequency domain sine-gaussian lensed signal with $\gamma=0.1$ and $M=0.02$ (scaled to time) **(Middle -One)**, Time domain sine-gaussian unlensed signal **(Middle -Two)**, Time domain sine-gaussian lensed signal **(Bottom)** Here y-axis is in dimensionless.

This will generate lensed sine-gaussian signal in frequency domain. These can be visualized back in time domain by performing one-dimensional Inverse Fast Fourier Transform of the real input (IRFFT) as follows:

$$H_+^{SG \text{ lensed}}(t) = \sqrt{2f_s T_{obs}} \text{irfft}(h_+^{SG \text{ lensed}}(f)) \quad (4.5)$$

$$H_\times^{SG \text{ lensed}}(t) = \sqrt{2f_s T_{obs}} \text{irfft}(h_\times^{SG \text{ lensed}}(f)) \quad (4.6)$$

where f_s and T_{obs} are the sampling frequency and duration of the signal respectively.

Figure 4.1 shows the time domain and frequency domain sine-gaussian signal along with the interferometer noises from LIGO added before and after gravitational lensing from a mass that follows point mass distribution model.

Table 4.1 tabulates the properties of the sine-gaussian signal that is modelled to study point mass lens model and gravitational lensing effects produced by it.

Parameters	Sine-Gaussian signal	Point mass lens	Signal-to-Noise-Ratio	
			Optimal SNR	Matched Filter SNR LIGO-Hanford
A	5×10^{-22}		9.83	11.34+i0.61
f₀	50 Hz			
τ	0.02			
φ	0			
γ		0.1	28.62	29.10-i0.10
M		0.02 s (~4000 M _⊙)		

Table 4.1: Tabulation of lensing and signal parameters along with lensed and unlensed SNR values used for the study

We can see clearly from the table that the SNR values have improved for unlensed signal because it has been magnified due to the point mass lens model.

4.2 Binary Black Hole merger Gravitational wave signal

In order to generate a source signal that models a binary black hole (further referred as BBH) merger GW event (Broadhurst 2019), just like the case of sine-gaussian signal, we define a function outside the scope of Bilby (say, `gen_bbh`). This function will take parameters of binary black hole mergers as arguments such as individual masses of the black holes, their spins, their sky positions, luminosity distances, inclination angle with the observer, geocentric time etc.

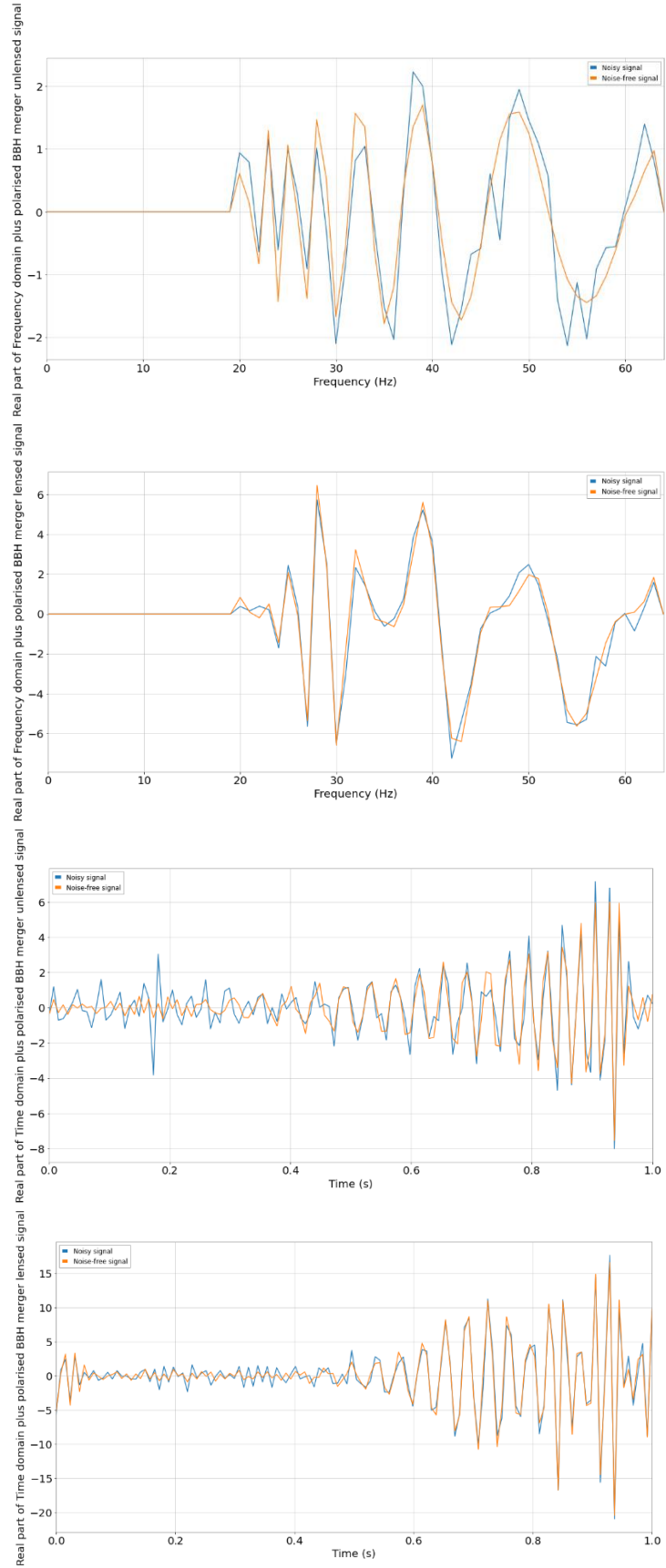


Figure 4.2: Frequency domain BBH merger GW unlensed signal at a frequency of $f_0=50\text{Hz}$ (**Top**), Frequency domain BBH merger GW lensed signal with $\gamma=0.1$ and $M=4000 M_\odot$ (**Middle -One**), Time domain BBH merger GW unlensed signal (**Middle -Two**), Time domain BBH merger GW lensed signal (**Bottom**) Here y-axis is dimensionless.

Inside the function, we also use sampling frequency and observation time to generate the BBH merger signal. A special function defined in LALsuite library called SimInspiralChooseFDWaveform is used to generate the frequency domain waveform of two black holes merging and producing compact binary coalescence gravitational wave signal. This function takes arguments such as mass of the two black holes, their sky positions, distance between the observer and the source (in this case, interferometer and the two black holes), inclination angle between the observer and the merging black holes, angle between the two black holes, minimum frequency of observation, maximum frequency of observation which according to Nyquist-Shannon sampling theorem should be lesser than or equal to $f_s/2$ where f_s is the sampling frequency that will be used by Bilby parameter estimator.

This pre-defined function will return a structure of plus and cross polarization strain data of the binary black hole merger GW event. (Abbott 2016) This will generate a waveform that can further be passed on to the LIGO interferometers to create a simulated noise form to be added to the BBH merger signal.

Parameters	BBH merger signal	Point mass lens	Signal-to-Noise-Ratio	
			Optimal SNR	Matched Filter SNR LIGO-Livingston
M_1	36.0 M_\odot		12.10	11.70+i0.49
M_2	29.0 M_\odot			
D_L	500 Mpc			
Θ_{jn}	150°			
ϕ	0°			
y		0.1	28.91	27.24+i0.51
M_L		4000 M_\odot		

Table 4.2: Tabulation of lensing and GW signal parameters along with lensed and unlensed SNR values used for the study

Figure 4.2 shows the time domain and frequency domain BBH merger GW signal along with the interferometer noises from LIGO-Livingston added before and after gravitational lensing from a mass that follows point mass distribution model. Table 4.2 tabulates the properties of the GW signal from the two merging black holes that is modelled to study point mass lens model and gravitational lensing effects produced by it. We can see clearly from the table that the SNR values have improved for unlensed signal because it has been magnified due to the point mass lens model.

Chapter 5

Results & Analysis

In this chapter, we will present the results obtained from parameter estimation of signal and lensing parameters for both sine-gaussian and BBH merger models. We will analyze how each signal parameter is affected by the lensing parameters and what effect does the point mass lens object between the source and the observer produce on the signal.

In the latter part of this chapter, we will focus more on strong and weak lensing, transition between wave and geometric optics limit, what happens when we estimate the signal at the recovery by not considering the lensing effect that has been created on the source signal side. Several interpretations based on each module is briefed throughout this chapter under discussions.

5.1 Source signal parameters before lensing by the Point-mass object

5.1.1 Sine-Gaussian signal

While recovering the signal for parameter estimation, we perform dynesty – a dynamic nested sampling algorithm to produce multi-dimensional samples drawn from the posterior distribution on the parameters based on the prior range defined for the parameter. The dynesty sampler runs until the remaining logarithmic evidence ($d\log z$) estimates to a value below 0.1 (default). In this source signal, 7983 samples are generated and corner plot and histogram for the input parameters amplitude A and central frequency f_0 is produced as shown in Figure 5.1. In this model, we get a \log_e evidence of -240.050 ± 0.085 and \log_e Bayes factor of 112.600 ± 0.085 .

Parameters	Prior Ranges and functions	Posterior (99.7% credible interval)
	Sine-Gaussian signal	Sine-Gaussian signal
A	10^{-23} - 10^{-21} (Log_e Uniform)	$5^{+2}_{-2} \times 10^{-22}$
f_0 (Hz)	40 – 60 (Uniform)	$49.15^{+3.07}_{-3.10}$
τ	0.02	-
ϕ	0	-

Table 5.1: Prior and posterior value of the unlensed sine-gaussian signal parameters

A tabulation of prior ranges and 99.7% credible interval with posterior values with highest likelihood is presented in Table 5.1. The quoted credible interval is consistent with the true injected parameters. The width of the posterior gives you the precision of the measurement and consistency indicates that things didn't go wrong.

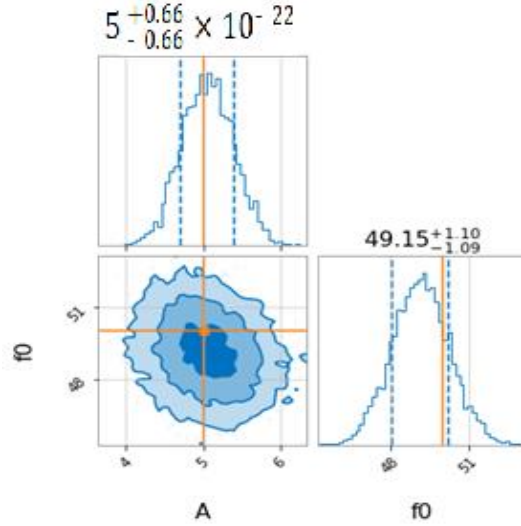


Figure 5.1: Corner plots for unlensed sine-gaussian signal parameters A and f_0 in Hz

From Figure 5.1 we can say that the amplitude of the sine-gaussian signal and the central frequency has a slight negative correlation between each other, and their histograms show the distribution of samples within approximately three standard deviation values.

5.1.2 BBH merger signal

We repeat the same procedure as we did for sine-gaussian curve, for the binary black hole merging gravitational wave signal. In this source signal, 16967 samples are generated and corner plot and histogram for the input parameters two individual masses of the black hole m_1 & m_2 and luminosity distance d_L is produced as shown in Figure 5.2. In this model, we get a \log_e evidence of -53.141 ± 0.158 and \log_e Bayes factor of 911.873 ± 0.158 .

It can be seen clearly from the corner plots generated by Bilby that both the masses of the black holes doesn't depend on the luminosity distance and thus, they are not correlated while the two masses have a strong negative correlation which means that if m_1 increases, m_2 decreases. This is predominantly because of the constraint we set of chirp mass and mass ratio of the two black holes. From basic knowledge on merging black holes, we know that the chirp mass is the resulting reduced mass of the compact binary black hole system after the merger and ringdown stage with the loss of mass explained as the result of energy loss by which the system emits gravitational waves that we measure using interferometers. Chirp mass of a two-body system is given by

$$\mathcal{M} = \left[\frac{(m_1 m_2)^{\frac{3}{5}}}{(m_1 + m_2)^{\frac{1}{5}}} \right] \quad (5.1)$$

when the component masses are equal to m_1 and m_2 . Since chirp mass determines how much energy is lost in the process of generating the gravitational wave, a constraint on this parameter is essential.

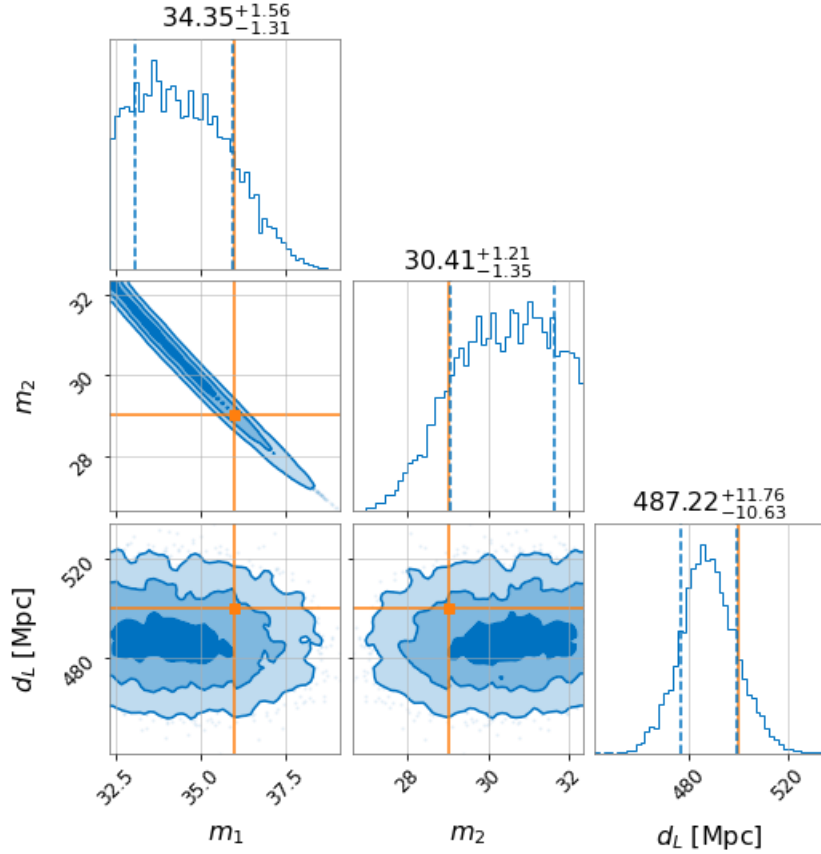


Figure 5.2: Corner plots for unlensed BBH signal parameters – two masses in M_{\odot} and luminosity distance in Mpc

The mass ratio is the ratio between the two masses, and we retain a constraint that it should always be lesser than unity because the mass of one black hole should never exceed the other though they have overlapping priors. The value of priors on each parameter and constraint range on chirp mass and mass ratio is tabulated in Table 5.2. This table also shows the posterior estimate and 99.7% confidence interval range for each parameter estimated in the corner plot.

Parameters	Prior Ranges and functions	Posterior (99.7% credible interval)
	BBH merger signal	BBH merger signal
$m_1 (M_{\odot})$	0.0-50.0 – Uniform	$34.35^{+4.68}_{-3.93}$
$m_2 (M_{\odot})$	0.0-50.0- Uniform	$30.41^{+3.63}_{-4.05}$
$D_L (Mpc)$	20-2000 – Power Law ($\alpha=2$)	$487.22^{+35.28}_{-31.89}$
Θ_{jn}	150°	-
ϕ	0°	-
Constraints:		
Chirp Mass (M_{\odot})	0.0-50.0	-
Mass Ratio	0.1-1.0	-

Table 5.2: Prior and posterior value of the unlensed BBH signal parameters

5.2 Source signal parameters after lensing by the Point-mass object

5.2.1 Sine-Gaussian signal

Now, we perform recovery of parameters for lensed sine-gaussian signal by sampling over the prior range of values for source signal parameters and lensing parameters which is tabulated in Table 5.3. In this lensed source signal, 14802 samples are generated, and we get a \log_e evidence of -244.827 ± 0.142 and \log_e Bayes factor of 905.846 ± 0.142 . The posterior values obtained as a result of dynamic nested sampling of the data over the prior range along with three standard deviation range around the maximum likelihood estimate of the parameter is also tabulated in Table 5.3.

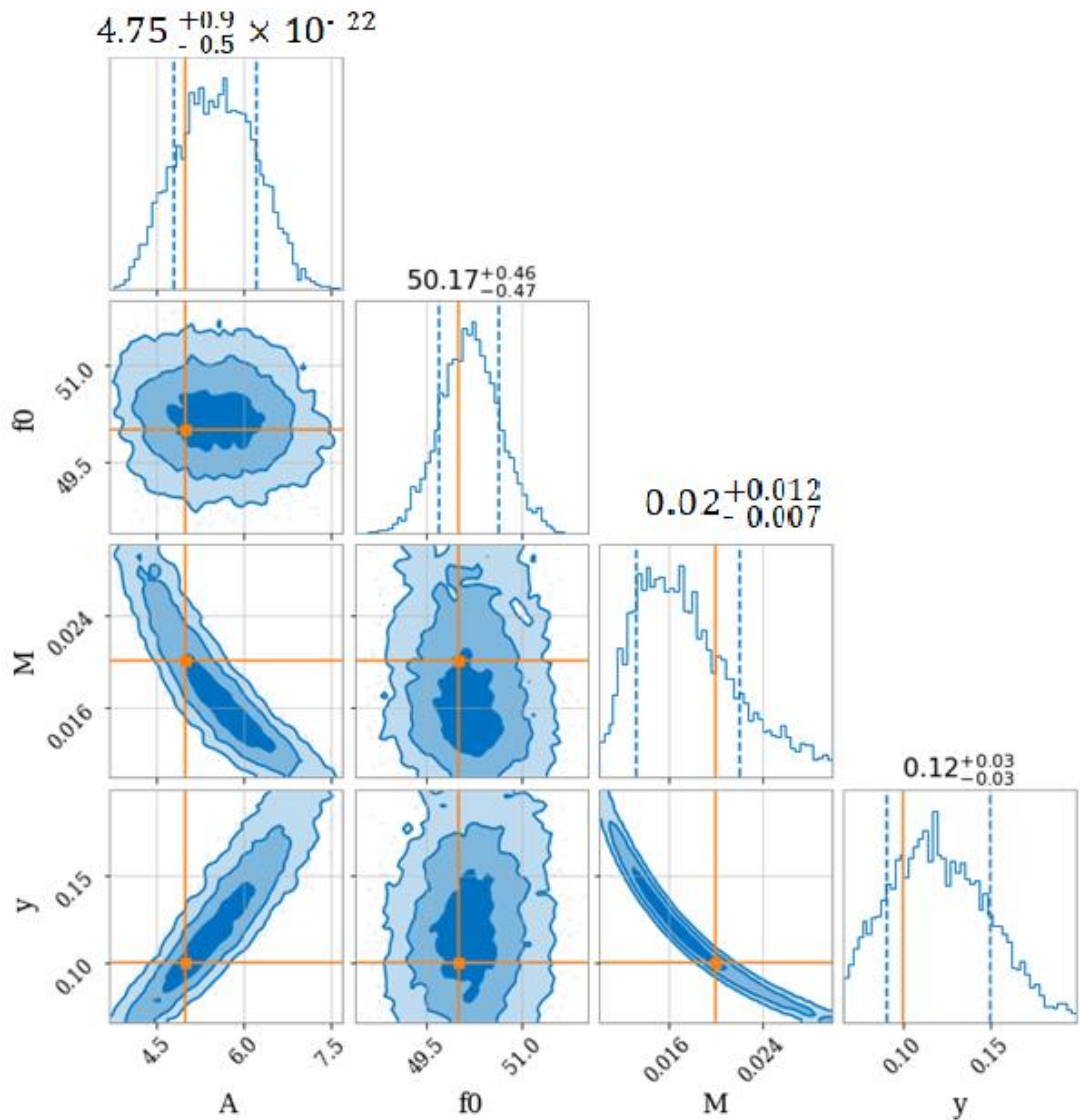


Figure 5.3: Corner plots for lensed sine-gaussian signal parameters A & f_0 (Hz) and lensing parameters y (dimensionless) & M (in M_\odot)

Parameters	Prior Ranges and functions		Posterior (99.7% credible interval)	
	Sine-Gaussian signal	Point mass lens	Sine-Gaussian signal	Point mass lens
A	10^{-23} - 10^{-21} (Log_e Uniform)		$4.75^{+2.8}_{-1.5} \times 10^{-22}$	
f_0 (Hz)	40 – 60 (Uniform)		$50.17^{+1.38}_{-1.41}$	
τ	0.02		-	
ϕ	0		-	
y		0.01-0.3 - Uniform		$0.12^{+0.09}_{-0.09}$
M_L (s)		0.01 – 0.05 - Uniform (2000 - 10000 M_\odot)		$0.02^{+0.03}_{-0.02}$

Table 5.3: Prior and posterior value of the lensed sine-gaussian signal and lensing parameters

For the sine-gaussian lensed signal, we assign delta function priors on τ and ϕ while estimate amplitude A and central frequency f_0 over a definite prior range that logarithmically uniform in A and uniform over f_0 . Similarly, we set uniform priors over a definite range for the lensing parameters as well. The resulting corner plots and histogram for each of the lensing and signal parameters is shown in Figure 5.3.

We can see from Figure 5.3 that the slight negative correlation we observed between amplitude and frequency in unlensed signal has disappeared in lensed signal case and the 99.7% credible region has reduced in range for frequency which could be the reason that in lensed sine gaussian signal, there is no correlation between the amplitude and frequency i.e., as the amplitude varies over its prior range, frequency remains approximately the same. We also observe that there is zero correlation between the central frequency and lensing parameters e.g., source offset y and lens mass (time-scaled) M i.e., as the value of y and M varies (increases or decreases), the central frequency of the sine-gaussian signal remains unchanged.

However, the amplitude of the sine-gaussian signal is heavily correlated with the lensing parameters. There exists a perfect positive correlation between the amplitude of the source signal and source position y . This can be interpreted as when the source is closer to being in-line with the lens object, the amplitude of the source signal increases which is an expected behavior. From the lens equation and plots made for amplification factor, we know that the magnification is more when the source offset is less.

We observe a strong negative correlation between the amplitude of the sine-gaussian signal and lens mass (scaled to time – multiplied by a factor of G/c^3). This leads to an inference that when the mass of the compact lens object (point-like mass) is more, the amplitude of the source signal decreases which means that the magnification due to lensing is less in this case. Note that, all these models are produced and evaluated in wave

optics limit only.

5.2.2 BBH merger signal

Now, we perform recovery of parameters for lensed binary black hole signal by sampling over the prior range of values for GW signal parameters and lensing parameters which is tabulated in Table 5.4. In this lensed GW source signal, 13875 samples are generated, and we get a \log_e evidence of -137.158 ± 0.136 and \log_e Bayes factor of 260.839 ± 0.136 . The posterior values obtained as a result of dynamic nested sampling of the data over the prior range along with three standard deviation range around the maximum likelihood estimate of the random variable is also tabulated in Table 5.4.

Parameters	Prior Ranges and functions		Posterior (99.7% credible interval)	
	BBH merger signal	Point mass lens	BBH merger signal	Point mass lens
$m_1 (M_\odot)$	0.0-50.0 - Uniform		$34.66^{+2.76}_{-4.05}$	
$m_2 (M_\odot)$	0.0-50.0 - Uniform		$30.13^{+3.69}_{-2.34}$	
$D_L (Mpc)$	20-2000 - Power Law ($\alpha=2$)		$486.76^{+163.95}_{-120.84}$	
θ_{jn}	150°		-	
Φ	0°		-	
Constraints:				
Chirp Mass (M_\odot)	0.0-50.0 - Uniform		-	
Mass Ratio	0.1-1.0 - Uniform		-	
γ	0.01-0.3 - Uniform		$0.11^{+0.06}_{-0.06}$	
$M_L (M_\odot)$	2000-6000 - Uniform		$3748.21^{+2847.81}_{-1944.18}$	

Table 5.4: Prior and posterior value of the lensed BBH signal and lensing parameters

From the table, we also see that the prior range on luminosity distance has increased by four to five folds. This increase in standard deviation of luminosity distance can be attributed to the increase in the magnitude or strength of the gravitational wave signal because of the magnification provided by the point mass lens model. The resulting corner plots and histogram for each of the lensing and signal parameters is shown in Figure 5.4.

Just like the corner plots obtained from the model of unlensed BBH merger event where the two masses of the compact black holes were independent of the distance parameter, they are also uncorrelated with the lensing parameters: the source offset γ and lens mass M whereas the two black hole masses are negatively correlated similar to the unlensed signal scenario.

Like the amplitude variable in sine-gaussian lensed waveform, the luminosity distance d_L is heavily correlated with the lensing parameters γ and M . This could be a possible explanation for the histogram of distance parameter to be spread out more than the unlensed waveform scenario.

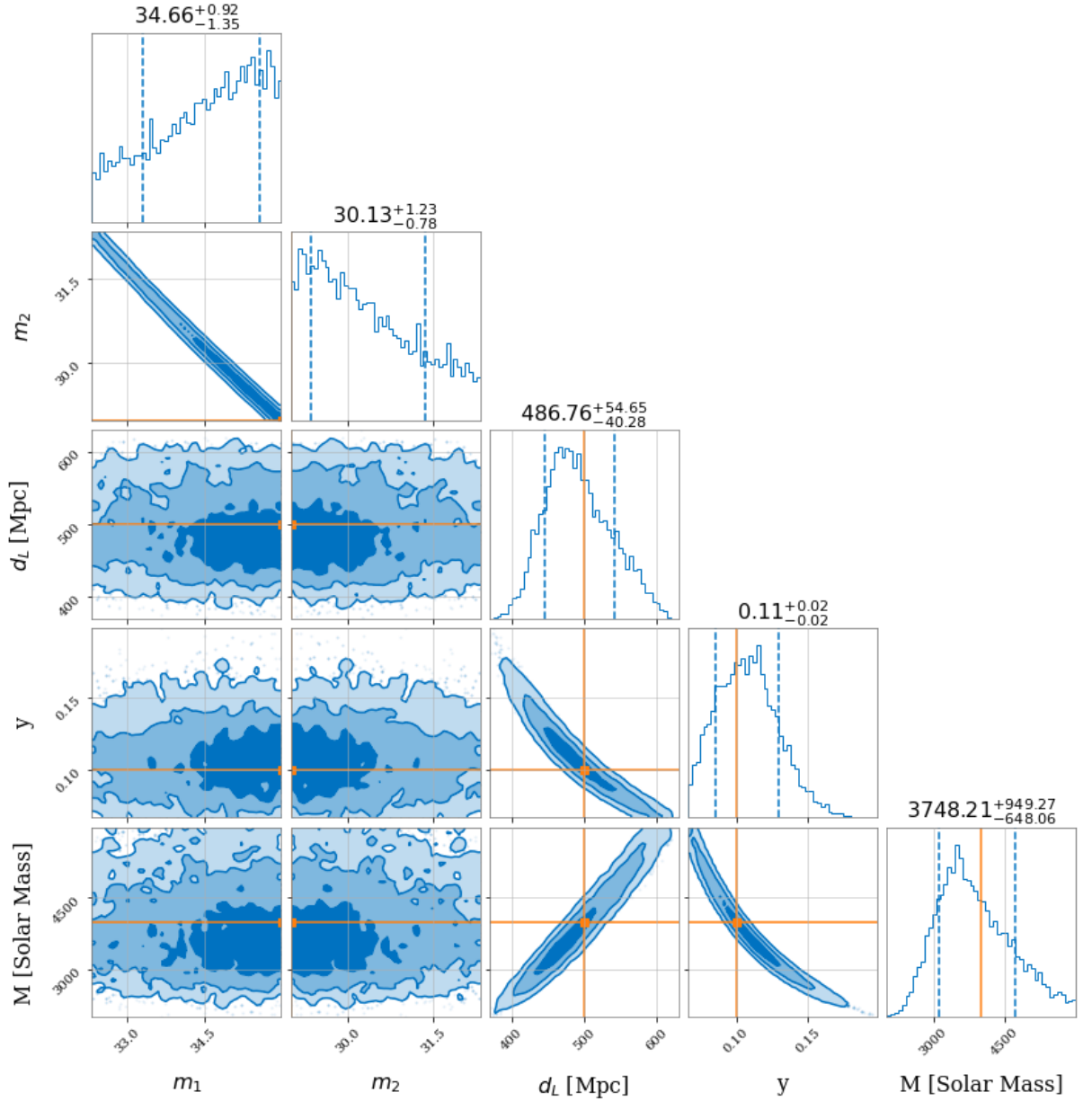


Figure 5.4: Corner plots for lensed BBH signal parameters m_1 , m_2 (in M_\odot) & d_L (in Mpc) and lensing parameters γ (dimensionless) & M (in M_\odot)

Luminosity distance or the distance between the source and the observer has strong positive correlation with the lens object's mass while it has an extremely perfect negative correlation with the source position γ . This is exactly to opposite to what we saw in the case of amplitude in sine-gaussian waveform. This is because, as the magnitude of amplification by lensing increases because of a decrease in source offset or increase in the mass of the point-like lens object, the distance from where the signal arrived can be assumed far because strong lensing could occur only when the source is distant because the probability of finding a heavy mass compact lens object is more in that case.

Like lensed sine-gaussian waveform, source position and lens mass take strong negative correlation as it is expected to be from the lens equation that describes the amplification factor as a function of dimensionless frequency and source position. From the corner plots, we can also observe that all the injection parameters lie within one standard deviation of

the posterior (64% confidence interval) that is estimated using nested sampling. This proves that the sampling has been performed correctly and the parameter estimation accurately matches with the source signal that we modelled.

5.3 Strong and weak gravitational lensing

Strong and weak lensing of gravitational waves are defined based on the values of source position and lens mass. When the lens mass is high (eg., mass of an SMBH) and the source position factor is low (~ 0.1), almost in line with the lens, then the resulting amplification due to lensing effects is very large and this results in strong lensing of the gravitational wave, wherein the SNR of the signal increases heavily and amplitude of the signal increases by several folds. In case of strong lensing, the dependency of source parameters on lens' random variables will be more and accurate.

When the lens mass is less ($\sim 100 M_{\odot}$) (compactness reduces), and the source offset is more (~ 3.0), then the resulting lensing effect will be very less, and the phenomena can be described as weak lensing. In case of weak lensing, the dependency of source parameters on lens' random variables will be less and not very precise.

5.4 Sampling without considering the lens effect

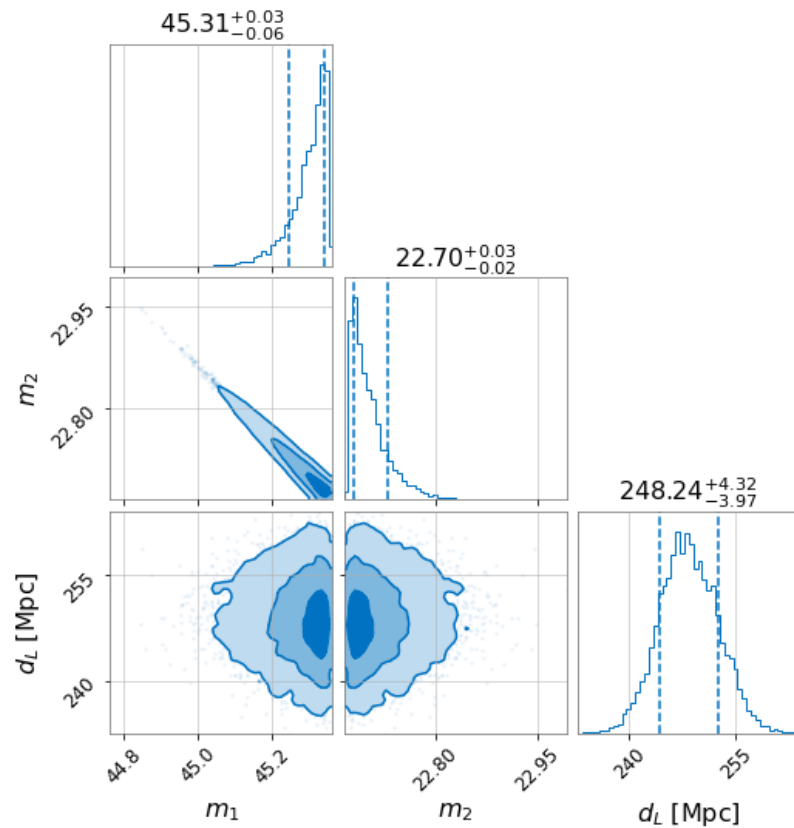


Figure 5.5: Corner plots for BBH merger GW signal which is lensed in the model, but the recovery samples ignore the lensing effects and estimate source signal parameters. m_1 and m_2 in M_{\odot} and d_L in Mpc

Let us consider the case where we create a strongly lensed signal with the properties as in

Table 5.4. During the recovery of the GW signal using dynesty sampler, we assume that there is no lensing, which is what LIGO and VIRGO does by default for any incoming signals over its three observing runs. Since we assume there is no lensing, we set uniform priors on the two black hole masses and the luminosity distance or distance between the source and the observer and the remaining parameters take delta priors equal to their injection values. For this GW source signal, 23002 samples are generated, and we get a \log_e evidence of -1443.188 ± 0.191 and \log_e Bayes factor of 1741.562 ± 0.191 .

The resulting corner plots when we assume that there is no lensing while sampling the input signal is shown in Figure 5.5. We can see from the figure that, just like the unlensed gravitational wave signal from binary black hole system, there is no correlation between the mass of the black holes and luminosity distance while there exists a negative correlation between the two masses of the black holes under study.

One important conclusion to note is that the posterior values of m_1 , m_2 and d_L are not equal to the injection values. There is huge offset in each value because we assume that there is no lensing. Primary black hole mass shows an increase in value than its injection value while secondary mass shows a decrease in its value than its original value. Though there existed no correlation between source masses and the lensing parameters, we observe that ignoring lens effects make us predict the wrong values of source masses. The luminosity distance value has dropped from 500 Mpc to ~ 250 Mpc. This offset can be easily explained because of the magnification in the signal due to lensing, the sampler assumes that it is close-by than its original distance because we ignore the fact that the signal is being lensed.

Chapter 6

Conclusion

6.1 Summary

This research discusses the gravitational lensing effects on gravitational wave signals from binary black hole merger system. In the process of working towards estimating the relationship between different parameters involved in a lensed gravitational wave signal, we make obtain few other results. These results are summarized as follows:

- A mathematical form of lens equation that describes the point mass lens model and singular isothermal sphere (SIS) lens model system is presented analytically. This analytic expression is used throughout the research in both geometric and wave optics limit.
- Magnitude and phase of the amplification factor for varying values of dimensionless frequency and source position is plotted and several inferences are made based on the oscillations produced by the amplification factor at higher values of w .
- A sine-gaussian source signal is produced for a certain frequency and point-mass lens model is attached to it. From the posterior distribution of the parameters several conclusions are made based on the source and lens' properties.
- Similarly, a merging binary black hole GW signal is produced, and the point-mass lens model is attached to it. The signal and lensing parameters are estimated using nested sampling and the resulting corner plot shows the correlation between the different parameters involved in a lensed binary black hole system.
- A transition point between wave and geometric optics limit is found for a lensing system where the source position is ~ 0.5 . Using this value, we vary lens mass between a high range and use both the limits to advantage and create a lensed BBH model.
- Strong and weak gravitational lensing based on varying the lens mass and source position is discussed and analyzed.
- Finally, the key results, wherein we recover the lensed BBH signal by assuming that there is no lensing and see huge offset between the posterior obtained and the actual injected values.

6.2 Conclusion

The objective of this research is to study how various source signal parameters get affected by the lensing parameters due to gravitational lensing of the gravitational wave signal under study. In this report, we quantitatively assess how the amplification factor is affected for varying values of source position and dimensionless frequency that directly depends on frequency of GW radiation and lens mass (time-scaled). We model a sine-gaussian signal for a center frequency and attach the lens equation to it. In this case, we observe that the amplitude of the signal is heavily correlated with lensing parameters whereas the central frequency remains unaffected by both the lens parameters and the other signal parameter. As a key part of our research, we model a binary black hole merger system that produces gravitational wave signal and attach point-mass lens equation to it. When we estimate the parameters involved in this model, we see no correlation between the lens mass and the remaining parameters in the system while strong positive correlation between the lens mass and luminosity distance and strong negative correlation between source position and distance between the observer and the source. We also study that optimal transition point in dimensionless frequency that allows smooth transit between wave and geometric optics limit which lies around 10.0. LIGO/VIRGO interferometers never account for lensing in the gravitational wave signal during sampling. Thus, we sample a lensed signal by ignoring the lensing effect to see what effect it has on the input parameters. We find huge offset in black hole masses and luminosity difference as a result of ignoring the lensing effect produced by the model. Thus, we can conclude that, gravitational lensing effects should be considered while observing for gravitational waves with high probability of lensing in the universe using future ground and space-based interferometers for accurate estimation of the physical properties of the gravitational wave sources.

6.3 Future scope of the research

This research can be repeated for the case of singular isothermal sphere lens model which produces higher magnification than the point-mass lens model. However, since the analytic form of SIS lens equation still consist of summation or integral expression, it will slow down the likelihood evaluation to be more than fraction of seconds in Bilby. This problem can be overcome by pre-estimating the lens equation for several different values of w and y and interpolating them. The resulting table of values can be called while inserting the lens model to the GW signal. Several other parameters like sky positions, inclination etc. can also be estimated from a lensed GW signal to see how it gets affected due to the attached lensing model. Strong and weak lensing process can be analyzed by varying the lensing parameters over a certain range. The lens model can also be attached to a real-time GW signal to see how the lensed form of such signals would look like and estimate the probability of those signals being lensed. We can find out how likely it is that a source would be lensed in the first place. We can determine the lensing parameter space that could be detectable in real-time scenario. We can convert the source offset factor y in real time values and estimate several distance parameters involved like distance between source and lens, lens and observer etc. A theoretical analysis of the same has been presented in Appendix C.

References

- [1] A. Einstein, "On the General Theory of Relativity," *Sitzungsber. Preuss. Akad. Wiss. Berlin (Math. Phys.)*, vol. 1915, pp. 778–786, 1915.
- [2] Abbott, B. & Abbott, R. & Abernathy, Matthew & Adhikari, R. & Anderson, S. & Arai, K. & Araya, M. & Barayoga, J. & Barish, B. & Berger, B. & Billingsley, Garilynn & Blackburn, Kent & Bork, R. & Brooks, AF & Cahillane, C. & Callister, T. & Cepeda, Cris & Chakraborty, Rijuparna & Chalermongsak, Tara & Szilagy, B., "Tests of General Relativity with GW150914", *Physical Review Letters*. 116, 2016.
- [3] Ashton G., et al., "BILBY: A User-friendly Bayesian Inference Library for Gravitational-wave Astronomy", *The Astrophysical Journal Supplement Series*, 241, 27, 2019.
- [4] B. P. Abbott et al. "GWTC-1: A Gravitational-Wave Transient Catalog of Compact Binary Mergers Observed by LIGO and Virgo during the First and Second Observing Runs", *Phys. Rev. X*, 9:031040, 2019.
- [5] B. P. Abbott, R. Abbott, T. D. Abbott, M. R. Abernathy, F. Acernese, K. Ackley, C. Adams, T. Adams, P. Addesso, R. X. Adhikari, et al., "Localization and broadband follow-up of the gravitational-wave transient gw150914," *The Astrophysical Journal*, vol. 826, p. L13, 2016.
- [6] B. Paczynski, "Gravitational microlensing by the galactic halo," *Astrophysical Journal*, vol. 304, p. 1-5, 1986.
- [7] Broadhurst, Tom & Diego, Jose & Smoot, George, "Twin LIGO/Virgo Detections of a Viable Gravitationally-Lensed Black Hole Merger", *arXiv: General Relativity and Quantum Cosmology*, 2019.
- [8] Diego, J. M., Hannuksela, O. A., Kelly, P. L., Pagano, G., Broadhurst, T., Kim, K., Li, T. G. F., and Smoot, G. F., "Observational signatures of microlensing in gravitational waves at LIGO/Virgo frequencies", *A&A*, 627: A130, 2019.
- [9] F. A. Asenjo and S. A. Hojman, "New non-linear modified massless klein-gordon equation," *The European Physical Journal C*, vol. 77, 2017.
- [10] F. De Paolis, G. Ingrosso, A. A. Nucita, and A. Qadir, "A note on gravitational wave lensing," *Astronomy & Astrophysics*, vol. 394, p. 749-752, 2002.
- [11] F. De Paolis, G. Ingrosso, and A. A. Nucita, "Astrophysical implications of gravitational microlensing of gravitational waves," *Astronomy & Astrophysics*, vol. 366, pp. 1065-1070, 2001.

- [12] Futamase T, Tomita K, “Gravitational Lensing and the High-Redshift Universe”, *Prog. of Theor. Phys. Suppl. No. 133 ed.*, 1999.
- [13] Higson E., Handley W., Hobson M., Lasenby A., “Dynamic nested sampling: an improved algorithm for parameter estimation and evidence calculation”, *Statistics and Computing*, 29, 891-913, 2019.
- [14] J. Aasi et al., “Advanced LIGO”, *Class. Quantum Grav.*, 32:074001, 2015.
- [15] K. Haris, Ajit Kumar Mehta, Sumit Kumar, Tejaswi Venumadhav, Parameswaran Ajith, “Identifying strongly lensed gravitational wave signals from binary black hole mergers”, arXiv: 1807.07062v1, 2018.
- [16] K. Liao, M. Biesiada, and X.-L. Fan, “The wave nature of continuous gravitational waves from microlensing,” *The Astrophysical Journal*, vol. 875, p. 139, 2019.
- [17] Kip S Thorne, “The theory of gravitational radiation-an introductory review”, in *Gravitational radiation*, pages 1–57, 1983.
- [18] Kirsty J. Rhook, J. Stuart B. Wyithe, “Realistic event rates for detection of supermassive black hole coalescence by LISA”, *Monthly Notices of the Royal Astronomical Society*, Volume 361, Issue 4, August 2005, Pages 1145–1152, 2005.
- [19] LIGO Scientific Collaboration. LIGO Algorithm Library - LALSuite. free software (GPL), 2018.
- [20] M. Abramowitz and I. Stegun, *Handbook of Mathematical Functions with Formulas, Graphs, and Mathematical Tables*, vol. 55, n. 1972. U.S. Government Printing Office, 1970.
- [21] M Coleman Miller, “Intermediate-mass black holes as LISA sources”, *Institute of Physics*, Vol. 29, No. 9, 2009.
- [22] Magnus W, Oberhettinger F, Soni R P, “Formulas and Theorems for the Special Functions of Mathematical Physics”, Springer Verlag: New York, 1996.
- [23] Mclsaac, Connor, David Keitel, Thomas S. Collett, Ian W. Harry, Simone Mozzon, Oliver Edy and David Bacon, “Search for strongly lensed counterpart images of binary black hole mergers in the first two LIGO observing runs”, arXiv: General Relativity and Quantum Cosmology, 2019.
- [24] Meena A. K., Bagla J. S., “Gravitational lensing of gravitational waves: wave nature and prospects for detection”, *MNRAS*, 1-8, 2019.

- [25] N. Matsunaga and K. Yamamoto, “The finite source size effect and wave optics in gravitational lensing,” *Journal of Cosmology and Astroparticle Physics*, vol. 2006, pp. 023–023, 2006.
- [26] Nakamura T. T., “Gravitational lensing of gravitational waves from inspiraling binaries by a point mass lens by a point mass lens”, *Physical Review Letters*, 80, 1138-1141, 1997.
- [27] R. Takahashi and T. Nakamura, “Wave effects in the gravitational lensing of gravitational waves from chirping binaries,” *The Astrophysical Journal*, vol. 595, pp. 1039–1051, 2003.
- [28] Ruffa, A. A., “Gravitational Lensing of Gravitational Waves”, *The Astrophysical Journal*, 517, L31, 1999.
- [29] Schneider, P., Ehlers, J., & Falco, E. E., “Gravitational Lenses”, New York : Springer, 1992.
- [30] Singer, Leo & Goldstein, Daniel & Bloom, Joshua, “The Two LIGO/Virgo Binary Black Hole Mergers on 2019 August 28 Were Not Strongly Lensed”, arXIV, 2019.
- [31] Speagle J., Barbary K., “dynesty: Dynamic Nested Sampling package”, *Astrophysics Source Code Library*, 2018.
- [32] T. R., “Quasi-geometrical optics approximation in gravitational lensing,” *A&A*, vol. 423, no. 03, pp. 787–792, 2006.
- [33] Takahiro T. Nakamura, Shuji Deguchi, “Wave Optics in Gravitational Lensing”, *Progress of Theoretical Physics Supplement*, Volume 133, Pages 137–153, 1999.
- [34] V. Bozza, & L. Mancini, “Observing gravitational lensing effects by Sgr A* with GRAVITY”, *The Astrophysical Journal*, 753, 56, 2012.
- [35] Varma, Vijay & Ajith, Parameswaran, “Effects of non-quadrupole modes in the detection and parameter estimation of black hole binaries with nonprecessing spins”, *Physical Review D*. 96. 10.1103/PhysRevD.96.124024, 2016.
- [36] X.-D. Luo and W.-C. Lin, “Some new properties of confluent hypergeometric functions”, 2015.
- [37] Zhao H-S, Taylor J E, Silk J, Hooper D, Mini-dark halos with intermediate mass black holes, *Phys. Rev. Letters*, 95, 011301, 2005.

Appendices

Appendix A

As explained in the main text, we know that the maximum value of amplification factor (or precisely, maximum amplification due to gravitational lensing of gravitational waves in wave optics limit) can occur only when the source offset is less or tends to zero. Thus, deriving the value of the amplification factor at $y=0$ can prove to be useful.

A.1 Derivation of equation (2.15)

Amplification factor of Point mass lens at $y=0$

We know that, equation (2.14) gives the value of amplification factor for any specific value of dimensionless frequency and source position for a point mass lens model. This is the lens equation for the model.

$$F_w(w, y) = \exp\left[\frac{i}{2}w(y^2 + \log\left(\frac{w}{2}\right))\right] \exp\left(\frac{\pi}{4}w\right) \Gamma\left(1 - \frac{i}{2}w\right) {}_1F_1\left(1 - \frac{i}{2}w, 1; -\frac{i}{2}wy^2\right) \quad (\text{A.1})$$

Using the mathematical identity $|\Gamma(1 + ai)|^2 = a\pi/\sinh(a\pi)$ from Abramowitz and Stegun 1972, we can say that

$$\left|\Gamma\left(1 - \frac{w}{2}i\right)\right|^2 = \frac{\frac{-w}{2}\pi}{\frac{\exp\left(\frac{-w\pi}{2}\right) - \exp\left(\frac{w\pi}{2}\right)}{2}} \quad (\text{A.2})$$

$$= \frac{w\pi}{1 - \exp(-w\pi)} \exp\left(-\frac{w\pi}{2}\right) \quad (\text{A.3})$$

Inserting this equation in (A.1) and taking the absolute value on both sides, we get,

$$|F_w(w, y)| = \left| \exp\left(\frac{\pi}{4}w\right) \sqrt{\frac{w\pi}{1 - \exp(-w\pi)}} \exp\left(-\frac{w\pi}{4}\right) {}_1F_1\left(1 - \frac{i}{2}w, 1; -\frac{i}{2}wy^2\right) \right| \quad (\text{A.4})$$

Now after setting the source position $y=0$ and using the following identity as in Abramowitz and Stegun 1972,

$$\lim_{c \rightarrow 0} {}_1F_1(a, b; c) = 1 \quad (\text{A.5})$$

we get the final equation (2.15), as follows:

$$F_{wave,max}(w, y = 0) = \sqrt{\frac{\pi w}{1 - \exp(-\pi w)}} \quad (A.6)$$

We know that, in geometric optics limit, wherein dimensionless frequency is higher than unity, this equation reduces to the following form:

$$F_{geo,max}(w, y = 0) = \sqrt{\pi w} \quad (A.7)$$

Appendix B

B.1 Derivation of equation (2.22)

Amplification factor of Singular Isothermal Sphere lens at $y=0$

We know that, equation (2.14) gives the value of amplification factor for any specific value of dimensionless frequency and source position for a SIS lens model. This is the lens equation for the model.

$$F_w(w, y) = \exp\left[\frac{i}{2}wy^2\right] \sum_{n=0}^{\infty} \left\{2w \exp\left(i\frac{3\pi}{2}\right)\right\}^{\frac{n}{2}} \frac{\Gamma\left(1 + \frac{n}{2}\right)}{n!} {}_1F_1\left(1 + \frac{n}{2}, 1; -\frac{i}{2}wy^2\right) \quad (B.1)$$

When we solve for source position equal to zero, we get the following integral form of the lens equation:

$$\begin{aligned} F(w, 0) &= -iw \int_0^{\infty} x \exp\left(iw \left[\frac{1}{2}x^2 - x\right]\right) dx \\ &= -w \int_0^{\infty} t \exp\left(w \frac{1}{2}t^2 - i\frac{1}{2}wt\right) dt \end{aligned} \quad (B.2)$$

(Note that in the second step we have used change of variables method on the integral calculus where we use the new variable t as \sqrt{ix} .)

From Matsunaga 2006, we can reduce (B.2) into a simple form as follows:

$$F(w, 0) = \exp\left(\frac{i}{4}w\right) D_{-2}\left(\exp\frac{i3\pi}{4}\sqrt{w}\right) \quad (B.3)$$

where D_{-2} is the parabolic cylinder function that has the following definition:

$$D_{-2}(x) = \sqrt{\frac{\pi}{2}} \exp\left(\frac{x^2}{4}\right) \left(1 - \operatorname{Erf}\left(\frac{x}{\sqrt{2}}\right)\right) - \exp\left(\frac{-x^2}{4}\right) \quad (B.4)$$

Substituting (B.4) in (B.3), we get the maximum amplification factor value at $y=0$ as (2.22)

Appendix C

C.1 Source position parameter y in terms of physical lens parameter values

We know that the parameters x and y are dimensionless which means that since D_d and D_s are of same units (parsecs), η and ξ are of same units as well.

The equation for ξ is as follows:

$$\xi = \sqrt{\frac{4MD_d D_{ds}}{D_s}} \quad (C.1)$$

Therefore, when distances are expressed in units of time (by dividing them by the speed of light) and masses are assumed to be in units of time as well (by multiplying them by G/c^3) then, ξ is also in units of time. This implies that η is in units of time (because it's a distance vector).

To get the specific distance ξ representing the perpendicular source distance from the line passing through the detector and the lens, then we get,

$$\eta = \frac{y\xi D_s}{D_L} = y \sqrt{\frac{4MD_s D_{ds}}{D_d}} \quad (C.2)$$

Thus, in order to convert y back to physical parameter space, we can consider distance between lens and observer as a lensing parameter while D_s will simply be the luminosity distance parameter that we're already estimating as in Section 5.2.2 and D_{ds} will be the difference between D_d and D_s . Note that the lens mass, all the distances and η should be in units of time and x and y are dimensionless while using the equation (C.2).